

OPERATIONAL CONCEPT DEFINITION DOCUMENT

Peter J. McGregor¹

Research School of Astronomy and Astrophysics
 Institute of Advanced Studies
 Australian National University

Revision History

Revision No.	Author & Date	Approval & Date	Description
Revision 1	Peter J. McGregor 30 November 2001	Gary Da Costa 1 March 2002	Draft initial document.
Revision 2	Peter J. McGregor 5 March 2002	Jan van Harmelen 23 April 2002	Revised initial document.
Revision 3	Peter J. McGregor 23 July 2002	Jan van Harmelen 25 July 2002	Revised for CoDR.
Revision 4	Peter J. McGregor 30 April 2003	Jan van Harmelen 9 May 2003	Revised following CoDR

Contents

1 Purpose.....	5
2 Applicable Documents	5
3 List of Acronyms	5
4 Introduction.....	6
5 Instrument Description	6
5.1 Basic Instrument Parameters	6
5.2 Imager Description	6
5.2.1 Filter Wheels	7
5.2.2 Utility Wheel.....	8
5.2.3 Imager Detector	10

¹ With major contributions from Gary Da Costa, Michael Dopita, Paul Francis, Ken Freeman, Brian Schmidt, Chris Tinney, and Peter Wood.

5.2.4 Imager Quick Look Displays.....	10
5.2.5 Non-Common Path Phase Errors	10
5.2.6 Imager Sensitivities	10
5.2.7 Imager On-Detector Guide Window Sensitivities	14
5.2.8 Comments on Astrometric Precision.....	15
5.3 Cryostat and Auxiliary Systems.....	16
5.4 Satellite Interference.....	16
5.5 Gemini Systems	16
6 Science Drivers.....	16
6.1 Overview	16
6.2 The Orion Nebula - A Detailed Study of a Nearby Massive Star-Forming Region	17
6.2.1 Science Goal.....	17
6.2.2 Sensitivity Limit.....	17
6.2.3 Guide Star Availability.....	18
6.2.4 Special Requirements	18
6.3 Young Stellar Super-Clusters	19
6.3.1 Science Goal.....	19
6.3.2 Sensitivity Limit.....	19
6.3.3 Guide Star Availability.....	19
6.3.4 Special Requirements	20
6.4 White Dwarf Cooling Ages in Galactic Open Clusters.....	20
6.4.1 Science Goal.....	20
6.4.2 Sensitivity Limit.....	20
6.4.3 Guide Star Availability.....	20
6.4.4 Special Requirements	20
6.5 Globular Cluster Mass Functions Over a Range of Metallicities.....	20
6.5.1 Science Goal.....	20
6.5.2 Sensitivity Limit.....	20
6.5.3 Guide Star Availability.....	21
6.5.4 Special Requirements	21
6.6 Missing Mass in Magellanic Cloud Planetary Nebulae	21
6.6.1 Science Goal.....	21
6.6.2 Sensitivity Limit.....	21
6.6.3 Guide Star Availability.....	21
6.6.4 Special Requirements	22
6.7 Proper Motions of Local Group Galaxies.....	22
6.7.1 Science Goal.....	22
6.7.2 Sensitivity Limit.....	22
6.7.3 Guide Star Availability.....	22
6.7.4 Special Requirements	22
6.8 Stellar Populations in Dwarf Galaxies.....	22
6.8.1 Science Goal.....	22
6.8.2 Sensitivity Limit.....	23
6.8.3 Guide Star Availability.....	23
6.8.4 Special Requirements	23
6.9 Calibration of the Supernovae Ia Zeropoint.....	23

6.9.1 Science Goal.....	23
6.9.2 Sensitivity Limit.....	23
6.9.3 Guide Star Availability.....	23
6.9.4 Special Requirements.....	23
6.10 Intracluster Stars in Nearby Galaxy Clusters.....	24
6.10.1 Science Goal.....	24
6.10.2 Sensitivity Limit.....	24
6.11 Measuring H_0 Out to 60 Mpc Using Red Supergiants.....	24
6.11.1 Science Goal.....	24
6.11.2 Sensitivity Limit.....	24
6.11.3 Guide Star Availability.....	24
6.11.4 Special Requirements.....	24
6.12 Measuring the Bulk Motions of Galaxies to $cz < 6000$ km/s with Surface Brightness Fluctuations.....	24
6.12.1 Science Goal.....	24
6.12.2 Sensitivity Limit.....	24
6.12.3 Guide Star Availability.....	25
6.12.4 Special Requirements.....	25
6.13 The Formation of the Disks of Disk Galaxies.....	25
6.13.1 Science Goal.....	25
6.13.2 Sensitivity Limit.....	25
6.13.3 Guide Star Availability.....	25
6.13.4 Special Requirements.....	25
6.14 Color Gradients in High Redshift Field Galaxies.....	25
6.14.1 Science Goal.....	25
6.14.2 Sensitivity Limit.....	26
6.14.3 Guide Star Availability.....	26
6.14.4 Special Requirements.....	26
6.15 Exploring Dark Energy Via High Redshift Supernovae.....	26
6.15.1 Science Goal.....	26
6.15.2 Sensitivity Limit.....	26
6.15.3 Guide Star Availability.....	27
6.15.4 Special Requirements.....	27
7 Setup and Calibration Requirements.....	27
7.1 Daytime GSAOI Setup and Calibration.....	27
7.1.1 GSAOI Bias and Dark Frames.....	27
7.1.2 MCAO AOM Calibrations.....	28
7.1.3 GSAOI Flat Field Frames.....	28
7.1.4 MCAO Laser Startup.....	28
7.2 Nighttime GSAOI Setup and Calibration.....	29
7.2.1 Twilight GSAOI Flat Field Frames.....	29
7.2.2 Nighttime MCAO Calibration.....	29
7.2.3 Nighttime GSAOI Flux Calibration.....	29
7.2.4 Nighttime GSAOI Geometrical Distortion Calibration.....	29
7.3 MCAO Science Field Acquisition.....	29
7.4 Nightly Shutdown.....	30

7.4.1 GSAOI Shutdown.....	30
7.4.2 MCAO AOM Shutdown.....	30
7.4.3 MCAO Laser Shutdown.....	30
8 Observing Scenarios	30
8.1 Evolution of Dwarf Irregular Versus Elliptical Galaxies	30
8.1.1 Scientific Background	30
8.1.2 Proposed Observations	30
8.1.3 Planning the Observation.....	30
8.1.4 Daytime Calibrations	40
8.1.5 Nighttime Calibrations.....	43
8.1.6 Setup Prior to Observation	46
8.1.7 Science Observation Sequence.....	79
9 Summary of Scientific Requirements.....	122
9.1 MCAO Compatibility.....	125
9.2 Imager.....	128
9.3 Imager Wavelength Coverage	131
9.4 Imager Spatial Sampling	134
9.5 Imager Field-of-View.....	137
9.6 Imager Cold Stop	140
9.7 Imager Pupil Viewer	143
9.8 Imager Non-Common Path Phase Errors	146
9.9 Imager Filter Suite.....	149
9.10 Imager Calibration.....	177
9.11 Imager Pupil Viewer Resolution	180
9.12 Imager Strehl Ratio.....	183
9.13 Imager Distortion.....	188
9.14 Imager Throughput.....	191
9.15 Imager Instrumental Background.....	194
9.16 Imager Ghost Images.....	197
9.17 Imager Sensitivity.....	200
9.18 Imager Pupil Viewer Sensitivity	203
9.19 Mechanism Set Time.....	206
9.20 Mechanism Configuration Time	209
9.21 Imager Utility Wheel.....	212
9.22 Imager On-Detector Guide Window.....	222
9.23 Imager Detector Read Noise.....	225
9.24 Imager Detector Dark Current.....	228
9.25 Imager On-Detector Guide Window Performance	231
9.26 Downtime.....	236
9.27 Observing Modes.....	239
10 References	242

1 Purpose

This document describes the operational concept model for the Gemini South Adaptive Optics Imager (GSAOI). The document summarizes the science cases for which the instrument has been designed, relates these to the design requirements, and discusses the key functional and performance requirements that the instrument must meet. Key operational scenarios of the GSAOI instrument are identified and discussed, especially in terms of the requirements the instrument places on other parts of the Gemini system. These scenarios are described in sufficient detail for technically and scientifically skilled, but non-expert, readers to understand.

2 Applicable Documents

Document ID	Source	Title
	IGPO	Conceptual Design Review Documents, MCAO for Gemini-South
REV-AO-G0172	IGPO	MCAO for Gemini South Preliminary Design Report
RPT-AO-G0107	IGPO	The Science Case for the Multi-Conjugate Adaptive Optics System on the Gemini South Telescope Version 2.0

3 List of Acronyms

2MASS	Two Micron All Sky Survey
ACS	Advanced Camera for Surveys
ADC	Atmospheric Dispersion Corrector
AGB	Asymptotic Giant Branch
ALTAIR	Altitude-Conjugated Adaptive Optics for Infrared
AO	Adaptive Optics
AOM	Adaptive Optics Module
BS	Beam Splitter
BTO	Beam Transfer Optics
CCD	Charge Coupled Device
CDM	Cold Dark Matter
CM	Centering Mirror
CMD	Color-Magnitude Diagram
dE	Dwarf Elliptical
DM	Deformable Mirror
DSS	Digitized Sky Survey
DWFS	Diagnostic Wave Front Sensor
FWHM	Full Width at Half Maximum
GCAL	Gemini Calibration Unit
GNIRS	Gemini Near-InfraRed Spectrograph
GSAOI	Gemini South Adaptive Optics Imager
HAWAII	HgCdTe Astronomical Wide Area Infrared Imager
HST	Hubble Space Telescope
ICM	Intracluster Medium
IGPO	International Gemini Project Office
IMF	Initial Mass Function
IOC	Input-Output Controller
ISAAC	Infrared Spectrometer and Array Camera
ISS	Instrument Support Structure
KM	K-Mirror

LLT	Laser Launch Telescope
LMC	Large Magellanic Cloud
LS	Laser System
MBE	Molecular Beam Epitaxy
MCAO	Multi-Conjugate Adaptive Optics
MCAO-CS	MCAO Control System
NGS	Natural Guide Star
NICMOS	Near-Infrared Camera and Multi-Object Spectrograph
NIFS	Near-infrared Integral Field Spectrograph
NIRI	Near Infra-Red Imager
OAP	Off Axis Parabola
ODGW	On-Detector Guide Window
OIWFS	On-Instrument Wave Front Sensor
PDR	Preliminary Design Review
PM	Pointing Mirror
PNe	Planetary Nebulae
PSF	Point Spread Function
PWFS	Peripheral Wave Front Sensor
SALSA	Safe Aircraft Localization and Satellite Acquisition
SBF	Surface Brightness Fluctuation
SDSU	San Diego State University
SMC	Small Magellanic Cloud
SNe	Supernovae
TTM	Tip-Tilt Mirror
USNO	United States Naval Observatory
VLT	Very Large Telescope
WFPC2	Wide Field and Planetary Camera 2
WFS	Wave Front Sensor

4 Introduction

The Gemini 8-m telescopes are designed to achieve unprecedented ground-based image quality using adaptive optics (AO) techniques. This has been demonstrated with Hokupa'a on Gemini North, and with ALTAIR. These are classical AO systems that are restricted in their corrected fields and sky coverage. The Gemini South Multi-Conjugate Adaptive Optics (MCAO) system is being designed to overcome these limitations. MCAO will provide uniform, diffraction-limited image quality at near-infrared wavelengths across an extended field-of-view. Useful levels of atmospheric seeing correction will be achieved over a full two arc minute diameter field-of-view, the maximum possible with the Gemini telescope design. Sky coverage will also be comparable to the ALTAIR laser guide star (LGS) system, or somewhat superior to it. MCAO will use three deformable mirrors conjugated to distinct altitude ranges in the atmosphere. These will be driven with commands computed from wave front sensor measurements of five LGSs and three natural guide stars (NGSs). Mean zenith Strehl ratios of 0.2 at *J*, 0.4 at *H*, and 0.6 at *K* will be achieved in median seeing on Cerro Pachon over a one arc minute diameter field using bright NGSs. These will decline to 0.05 at *J*, 0.18 at *H*, and 0.39 at *K* at a zenith distance of 45°. The MCAO system will be able to operate with fewer than three NGSs but with reduced performance.

The Gemini South Adaptive Optics Imager (GSAOI) will be the workhorse instrument used with MCAO. GSAOI is a near-infrared, diffraction-limited, imaging system. The imager detector includes an On-Detector Guide Window that monitors slow tip-tilt variations due to flexure between MCAO and GSAOI. GSAOI has a single fixed-format camera with 0.02" pixels that Nyquist sample the 0.042" FWHM diffraction-limited images produced at 1.65 μm , but slightly under-samples the 0.032" FWHM images at *J*, and slightly over-samples the 0.057" FWHM images at *K*. GSAOI uses a mosaic of Rockwell HAWAII-2RG HgCdTe/CdZnTe Molecular Beam Epitaxy (MBE) detectors with 4080 \times 4080 18 μm pixels arranged

in four 2040×2040 quadrants each separated by 2.5 mm. Thus GSAOI records a square field-of-view 84.7" on a side. The GSAOI optics have stable and low distortion that permits high precision astrometric observations, which are limited in performance only by the stability of MCAO. A comprehensive suite of broad-band and narrow-band filters is available. GSAOI combines high throughput with excellent, uniform image quality to provide a high sensitivity MCAO imaging system.

Section 5 of this document contains a description of the GSAOI instrument. The science cases for which GSAOI has been designed are described in Section 6. Setup and calibration requirements for GSAOI are described in Section 7. Section 8 contains descriptions of observing scenarios. The scientific requirements that follow from these science programs are listed in Section 9.

5 Instrument Description

5.1 Basic Instrument Parameters

- Wavelength range: 0.9-2.4 μm .
- Pixel size: 0.02"×0.02" on sky.
- Broad-band filters: Z, J, H, Ks, K', K.
- Narrow-band filters: zero-redshift emission lines.
- Detector: 4080×4080 pixel Rockwell HAWAII-2RG HgCdTe/CdZnTe MBE mosaic, 18 μm pixels.
- On-Detector Guide Windows: User-selectable, one per detector mosaic quadrant.
- Pupil viewer: Inserted without disturbing imager optics.
- Curvature wave front sensor: Inserted without disturbing imager optics.

5.2 Imager Description

The imager is the GSAOI science path. The 2' diameter f/34 MCAO output field is directed to GSAOI by the science fold mirror in the Instrument Support Structure (ISS). The beam passes through the GSAOI cryostat window and the central 85"×85" square science field comes to focus 300 mm inside the cryostat at a field mask. The beam then passes through a doublet field lens and a four-element optical relay. The field lens forms a pupil image within the relay optics where the internal cold stop is located. Two filter wheels are located immediately in front of this cold stop. The relay reimages the focal plane onto the imager detector at a scale of 0.02"/pixel. A utility wheel allows a lens group to be positioned temporarily between the relay and the detector to record an image of the cold stop. This cold stop image is used to accurately align the cryostat with the MCAO exit pupil. Convex and concave lenses, also in the utility wheel, produce defocused star images at the detector. These images are used to measure static wave front phase errors that are nulled using the MCAO deformable mirror DM0.

5.2.1 Filter Wheels

The contents of the GSAOI filter wheels are listed in Table 2 and Table 3. These contain standard near-infrared broad-band filters and zero-redshift near-infrared emission- and absorption-line filters.

Table 2: Upper Filter Wheel Contents

Position	Filter	λ_c (μm)	$\Delta\lambda$ (μm)	50% cut on	50% cut off
1	Clear
2	Z	1.015	0.170	0.930	1.100
3	J	1.250	0.160	1.170	1.330
4	H	1.635	0.290	1.490	1.780
5	K'	2.120	0.340	1.950	2.290
6	Ks	2.150	0.320	1.990	2.310
7	K	2.200	0.340	2.030	2.370
8	J continuum	1.207	0.018	1.198	1.216
9	H continuum	1.570	0.024	1.558	1.582
10	CH ₄ (short)	1.580	0.100	1.530	1.630
11	CH ₄ (long)	1.690	0.100	1.640	1.740
12	Ks continuum	2.093	0.031	2.078	2.108
13	Kl continuum	2.270	0.034	2.253	2.287
14	Spare
15	Spare

Table 3: Lower Filter Wheel Contents

Position	Filter	λ_c (μm)	$\Delta\lambda$ (μm)	50% cut on	50% cut off
1	Clear
2	He I 1.0830 μm	1.083	0.016	1.075	1.091
3	H I P γ	1.094	0.011	1.089	1.100
4	H I P β	1.282	0.019	1.272	1.292
5	[Fe II] 1.644 μm	1.644	0.025	1.631	1.656
6	H ₂ O	2.000	0.080	1.960	2.040
7	He I (2p2s)	2.058	0.031	2.042	2.073
8	H ₂ 1-0 S(1)	2.122	0.032	2.106	2.138
9	H I Br γ	2.166	0.032	2.150	2.182
10	H ₂ 2-1 S(1)	2.248	0.034	2.231	2.265
11	CO $\Delta v=2$	2.360	0.080	2.320	2.400
12	Spare
13	Spare
14	Spare
15	Blocked

5.2.2 Utility Wheel

The contents of the utility wheel are listed in Table 5. The “Clear” position is used for routine imaging. The pupil viewer is used to accurately align the cold stop with the MCAO exit pupil and so minimize the background reaching the imager detector. The convex and concave defocus lenses produce defocused images that are used to derive static wave front phase errors at the imager detector. These phase errors are nulled using the MCAO deformable mirror DM0 (§5.2.5).

Table 5: Utility Wheel Contents

Position	Content
1	Clear
2	Pupil viewer
3	Convex defocus lens
4	Concave defocus lens

5.2.3 Imager Detector

The imager detector is a 4080×4080 pixel mosaic of four three-side buttable 2040×2040 pixel Rockwell HAWAII-2RG HgCdTe/CdZnTe MBE devices with 18 μm pixels. The four detectors are each separated by ~ 2.5 mm. An additional four rows and columns around the outer edge of each detector are not illuminated. These are read out as reference pixels. HAWAII-2RG devices have high quantum efficiency even at short wavelengths, low dark current, low remnance, and no significant on-chip amplifier glow (**TBD!**). The imager detector mosaic is read out in ~ 10 s through 16 video lines. Fowler sampling and correlated double-sampling readout methods are implemented. The minimum integration time is ~ 5 s using the correlated double-sampling readout method.

Each device also has a programmable rectangular On-Detector Guide Window (ODGW) capability. A guide window of either 8×8, 12×12, 16×16, or 32×32 pixels can be specified. This is then read out rapidly during the imager exposure to monitor tip-tilt and flexure variations directly on the imager detector. It will frequently be convenient to use the near-infrared images of the MCAO NGSs for this purpose.

5.2.4 Imager Quick Look Displays

It is envisaged that data from the imager detector will be presented in two Quick Look Displays; the View Mode Quick Look Display and the Observe Mode Quick Look Display. Temporary data will be obtained and displayed in View Mode, but not archived. Science data will be obtained and displayed in Observe Mode. Observe Mode data will be archived. This convention is adopted in the observing scenario descriptions in §8.

5.2.5 Non-Common Path Phase Errors

Imaging performance is improved if the MCAO deformable mirror that is conjugated to ground level (DM0) can be configured to correct non-common path wave front phase errors introduced by the GSAOI optics. Normally, the MCAO Diagnostic Wave Front Sensor is used to flatten the wave front exiting the MCAO system. It is preferable to ensure that the wave front reaching the imager detector is flat. This will be achieved by recording images on either side of focus and analyzing them in the manner described by Roddier& Roddier (1993). The light source for these images will be the MCAO NGS source simulator. This is a 5×5 grid of fiber-fed sources that will produce separated defocused images. The images will be defocused using the convex and concave defocus lenses in the GSAOI utility wheel. The images will be analyzed using the *ExtraFocal* program, and the coefficients of low-order Zernike polynomials characterizing the wave front error will be input to the MCAO system.

5.2.6 Imager Sensitivities

Imager sensitivity has been quantified using a model for the object and background signals and the estimated detector dark current (0.05 e/s/pix) and read noise (5 e using multiple reads). The model assumes a detector quantum efficiency of $\sim 80\%$ (Hall, priv. comm.). Background signals considered are airglow emission and thermal emission from the sky, telescope, MCAO system, cryostat window, and cryostat interior. Limiting magnitudes for a total on-source integration time of 1 hr in 0.4" seeing through a 0.08"×0.08" square aperture are listed for each filter in Table 6 along with the Strehl ratio that was assumed for that filter and the sky brightness that resulted.

Saturation magnitudes for each filter are also listed in Table 6. These are calculated for an assumed minimum integration time of 5 s and a detector full well depth of 50,000 e. The same 0.4" seeing and Strehl ratios listed in Table 6 apply. The faint broad-band saturation magnitudes present a calibration problem: faint near-infrared photometric standards typically have $K \sim 10\text{-}12$ mag (e.g., Persson et al. 1998). It will be necessary to read out only a sub-region of the imager detector so as not to saturate these standard stars. The brightest Persson et al. (1998) standards can be recorded in a 256×256 sub-region ($5.1'' \times 5.1''$) that is read out 32 times faster than the full array using a minimum integration time of 0.16 s (because only two outputs can be used instead of four).

Table 6: Imager Sensitivities (10:1 in 1 hr)

Filter	Limiting Magnitude (mag)	Saturation Magnitude (mag)	Assumed Strehl Ratio	Sky Brightness (mag/arcsec ²)
<i>Z</i>	25.6	14.8	0.2	17.1
<i>J</i>	24.1	13.9	0.2	14.9
<i>H</i>	24.1	14.0	0.4	14.0
<i>K'</i>	23.9	13.3	0.6	13.5
<i>K_s</i>	23.8	13.2	0.6	13.4
<i>K</i>	23.7	13.2	0.6	13.3
<i>J</i> continuum	23.1	11.7	0.2	15.0
<i>H</i> continuum	22.9	11.5	0.4	14.1
CH ₄ (short)	23.6	13.1	0.4	13.9
CH ₄ (long)	23.4	12.7	0.4	13.8
<i>K_s</i> continuum	22.7	10.9	0.6	13.6
<i>K_l</i> continuum	22.5	10.6	0.6	13.5
He I 1.0830 μm	23.7	12.0	0.2	16.1
H I P γ	23.5	11.5	0.2	16.2
H I P β	22.5	11.5	0.2	14.0
[Fe II] 1.644 μm	22.7	11.4	0.4	13.8
H ₂ O	23.3	11.8	0.6	13.9
He I (2s2p)	22.5	10.8	0.6	13.3
H ₂ 1-0 S(1)	22.6	10.8	0.6	13.4
H I Br γ	22.6	10.7	0.6	13.5
H ₂ 2-1 S(1)	22.5	10.6	0.6	13.5
CO ($\Delta v=2$)	22.4	11.2	0.6	12.6

Modeled background signals for each filter with an integration time of 600 s are listed in Table 7. The dark current is assumed to contribute 30 e/pix in this integration time. It is clear from Table 7 that airglow line emission dominates for all broad-band filters and most narrow-band filters. Thermal emission from the MCAO system makes a major contribution in the three broad *K* bands and is dominant in the longer wavelength narrow-band filters. These background signals ensure that GSAOI with a read noise of 10 e will be background limited in integration times > 15 s at *Z*, > 4 s at *H*, and > 2 s at *K*, and in integration times > 120 s with all narrow-band filters. Many narrow-band filters will be strongly background limited in this time.

Table 7: Imager Background Contributions (600 s)

Filter	Airglow (e/pix)	Sky Thermal (e/pix)	Telescope Thermal (e/pix)	MCAO Thermal (e/pix)	Window Thermal (e/pix)	Total (e/pix)
<i>Z</i>	3867	0	0	0	0	3897
<i>J</i>	17904	0	0	0	0	17934
<i>H</i>	39048	1	5	16	1	39101
<i>K'</i>	22167	378	2162	6652	428	31819
<i>K_s</i>	21285	447	2555	7860	507	32685
<i>K</i>	19069	1002	4249	13072	849	38273
<i>J</i> continuum	1807	0	0	0	0	1838
<i>H</i> continuum	3216	0	0	0	0	3246
CH ₄ (short)	15301	0	0	1	0	15332
CH ₄ (long)	14851	0	2	7	0	14891
<i>K_s</i> continuum	2468	13	106	327	21	2966
<i>K_I</i> continuum	430	107	579	1782	116	3045
He I 1.0830 μm	796	0	0	0	0	826
H I Pγ	462	0	0	0	0	492
H I Pβ	4611	0	0	0	0	4641
[Fe II] 1.644 μm	4045	0	0	1	0	4076
H ₂ O	4730	87	106	327	20	5302
He I (2s2p)	3183	45	74	230	15	3577
H ₂ 1-0 S(1)	3024	7	146	449	29	3685
H I Brγ	2285	15	221	680	44	3275
H ₂ 2-1 S(1)	946	63	484	1491	97	3112
CO Δv=2	251	1228	2718	8360	549	13134

5.2.7 Imager On-Detector Guide Window Sensitivities

The imager On-Detector Guide Window (ODGW) performance has been estimated using the imager performance model to generate star frames that have then been centroided and the RMS centroiding accuracy determined from 200 simulated guide star frames. Limiting magnitudes that achieve a centroiding accuracy of ~ 2 mas (i.e., 0.1 pix) in integration times of 0.01 s (i.e., when used as a MCAO NGS) and 30 s (i.e., when monitoring flexure variations) are listed for each broad-band filter in Table 8. Also listed are the magnitudes of stars that will just saturate the detector in these integration times.

Table 8: Imager ODGW Sensitivities (2 mas RMS)

Filter	Limiting Magnitude	Saturation Magnitude	Limiting Magnitude	Saturation Magnitude
	10 ms integration (mag)	10 ms integration (mag)	30 s integration (mag)	30 s integration (mag)
<i>Z</i>	15.1	8.0	22.7	16.7
<i>J</i>	14.2	7.1	21.2	15.8
<i>H</i>	14.5	7.3	21.0	16.0
<i>K'</i>	13.7	6.6	20.4	15.2
<i>K_s</i>	13.6	6.5	20.3	15.2
<i>K</i>	13.5	6.5	20.2	15.1
<i>J</i> continuum	12.0	4.6	20.0	13.5
<i>H</i> continuum	12.0	4.7	19.7	13.4
CH ₄ (short)	13.5	6.3	20.5	15.0
CH ₄ (long)	13.1	5.9	20.1	14.6
<i>K_s</i> continuum	11.2	4.1	19.1	12.7
<i>K_l</i> continuum	11.0	3.8	18.8	12.5
He I 1.0830 μm	12.3	5.3	20.6	13.8
H I P γ	11.9	4.6	20.2	13.2
H I P β	11.8	4.6	19.4	13.3
[Fe II] 1.644 μm	11.8	4.5	19.4	13.2
H ₂ O	12.3	5.1	19.8	13.8
He I (2s2p)	11.2	3.9	18.9	12.7
H ₂ 1-0 S(1)	11.3	4.1	19.0	12.8
H I Br γ	11.3	4.0	18.9	12.7
H ₂ 2-1 S(1)	11.0	3.8	18.9	12.6
CO $\Delta v=2$	11.6	4.4	18.8	13.2

The availability of faint guide stars at near-infrared wavelengths has been investigated by Spagna² for NGST. He tabulates cumulative star counts from which probabilities can be calculated that the 2' diameter MCAO field for any science object will contain at least one guide star brighter than a particular limit. These probabilities are plotted in Figure 1 where it can be seen that the probability of finding at least one $K \leq 13$ mag guide star, suitable for use as a MCAO NGS with the broad-band filters, in the MCAO field is > 11% while the probability of finding at least one $K \leq 20$ mag guide star, suitable for flexure monitoring with the broad-band filters, in the MCAO field is high (> 97%).

² http://www.ngst.nasa.gov/public/unconfigured/doc_0422/rev_03/NGST_GS_report5.pdf

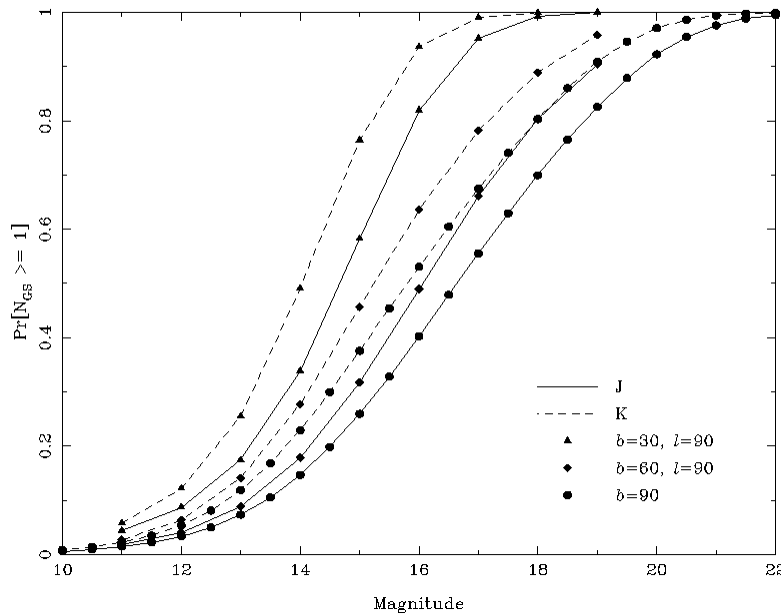


Figure 1: Guide star acquisition probabilities at J (solid lines) and K (dashed lines) for Galactic latitudes of 30° (triangles), 60° (diamonds), and 90° (circles).

5.2.8 Comments on Astrometric Precision

High precision astrometry will be a prominent application of MCAO and GSAOI. Differential astrometric techniques with CCDs have been shown to be extremely powerful. As long as the targets observed are unresolved (i.e., are stars), the precision with which the differential position of an object can be measured is limited only by the signal-to-noise ratio achieved and the long-term stability of the instrument in question. Astrometric programs on 2 to 4 m telescopes are routinely measuring differential object positions to 1/500th of a FWHM (Tinney 1996; Tinney et al. 1995; Monet et al. 1992).

The improved resolution offered by MCAO, the removal of differential seeing effects, and the operation of the GSAOI instrument in the infrared offer prospects for a dramatic improvement in the quality of ground-based differential astrometry.

Differential seeing is the crucial factor in determining the precision of ground-based differential astrometry. Over any field-of-view, the motions of different objects due to the atmosphere are different and become increasingly different at larger separations. Differential seeing effects always remain, even though the measured positions of targets average over time towards the underlying 'true' position (in the absence of the atmosphere). The dramatic improvement in differential seeing achieved by MCAO should significantly lower this systematic limitation, opening the way for a major breakthrough of the 1mas precision barrier by GSAOI.

Remaining systematic effects to be dealt with are differential atmospheric refraction and differential atmospheric color refraction. These impose limitations on the observing strategy (essentially observing only within ~ 1 hr of the meridian, and observing all epochs at near identical hour angles), but otherwise do not impact on scientific performance.

The photon-counting requirements for high precision astrometry remain: for a 50 mas FWHM observation at H band, measurement of a $500 \mu\text{as}$ position is possible with signal-to-noise ratio of 100, corresponding to $H \sim 21.6$ mag in 1 hr, and of a $160 \mu\text{as}$ position at $H = 21.6$ mag in ~ 10 hr.

These precisions are unprecedented for objects of these magnitudes. Astrometry at this level can; confirm or deny the membership of faint members of galactic open and globular clusters; obtain parallaxes for targets inaccessible due to their faintness, redness, or extinction to GAIA; measure the proper motions of most of the Local Group galaxies over a period of 5-10 yr. Some of these specific scientific issues are addressed in the science driver descriptions presented in §6.

5.3 Cryostat and Auxiliary Systems

GSAOI is a fast-tracked instrument that is intended to be available for MCAO commissioning. Duplicates of the NIRI/NIFS cryostat, integration frame, instrument control system, and control software will be used to reduce development time (Figure 4).

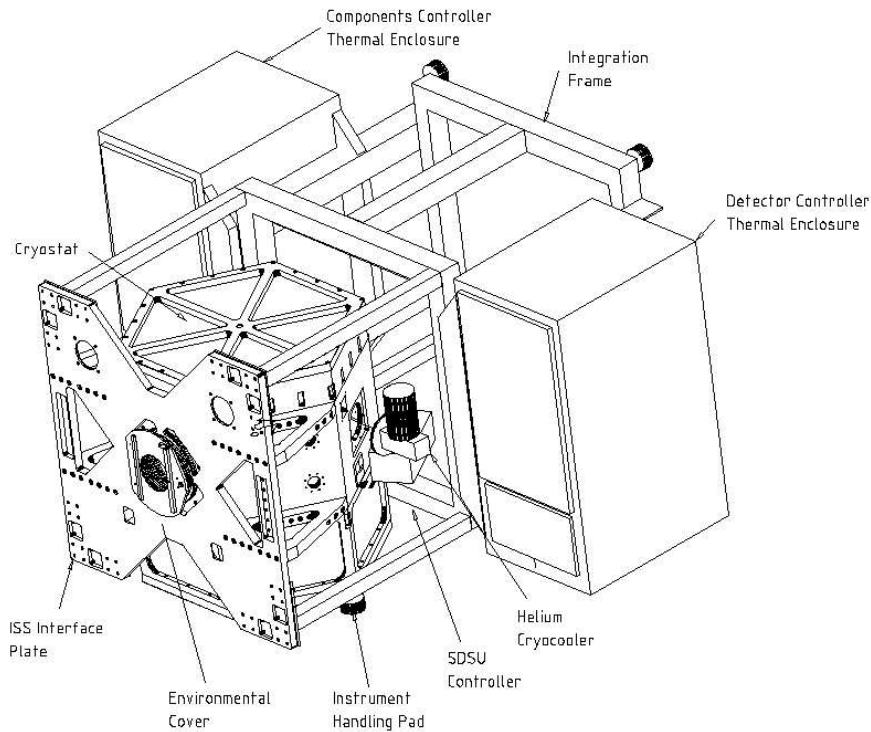


Figure 4: GSAOI cryostat, ISS interface plate, integration frame, and thermal enclosures.

The cryostat is a hexagonal cylinder 1.0 m in diameter and 1.3 m long. The circular cryostat window has been enlarged to accommodate the 2 arc minute diameter $f/34$ MCAO field. The exterior of GSAOI is similar to NIRI and NIFS in other ways. An environmental cover is located in front of the cryostat window to protect it and prevent dust accumulation when GSAOI is not in use. The cryostat mounts on the ISS via the ISS interface plate. The SDSU-2 controller used to control the GSAOI detector mounts directly on the outside of the cryostat. All other electronics are located in two thermal enclosures.

The two thermal enclosures are carried on the integration frame. One thermal enclosure contains the mechanism and temperature control electronics and the Instrument Control System Input-Output Controller (IOC). The second thermal enclosure contains the SDSU-2 power supply and the Detector Control System

³ http://www.ngst.nasa.gov/public/unconfigured/doc_0422/rev_03/NGST_GS_report5.pdf

IOC. The integration frame mounts on the ISS interface plate along with the cryostat but does not load the cryostat.

5.4 Satellite Interference

A laser beacon is not permitted to interfere with satellites, either by causing damage or by corrupting data from the satellite. A Laser Clearing House must vet proposed observations and allocate observing windows. These observing windows are typically shorter than 15 min duration. Consequently, science observations must either be limited to the available observing window, or they must be interrupted and the laser beam shut off when an observing window is not available. There should be no signal-to-noise ratio penalty for interrupting background-limited imaging observations in this way (see §5.2.6). However, measuring accurate median sky frames may prove problematic for severe disrupted observations.

The laser beam must also be shut off when the beam crosses the field-of-view of a neighboring telescope (which is expected to occur approximately once per night), and when the MCAO Safe Aircraft Localization and Satellite Acquisition (SALSA) system detects the presence of an aircraft. Generally, the GSAOI exposure will have to be aborted under such circumstances.

5.5 Gemini Systems

Use of MCAO with GSAOI imposes several restrictions on the use of other Gemini systems.

- The ISS AO fold mirror must be deployed to use MCAO. This means that PWFS2 cannot also be deployed.
- The ISS science fold mirror is used to direct light from GCAL to the science instrument. This light does not pass through MCAO so is unsuitable for flat field calibration of GSAOI.
- The acquisition camera can be used to define accurate relative coordinates of suitable GSAOI ODGW and MCAO NGSs.
- It is desirable to have the ability to insert a matrix mask within the MCAO system at the first telescope focal plane. This would be used to calibrate astrometric distortion in the whole MCAO/GSAOI optical train.
- MCAO should issue an abort command to GSAOI when the lasers are switched off in response to a SALSA alert. GSAOI should respond by aborting the current exposure.
- Read out of the ODGW stops while the initial and final full-frame read outs of the imager detector occur. The MCAO supervisory control loop must react benignly to this loss of ODGW signal so that the ODGW guide star remains near its correct position when ODGW read outs resume.

6 Science Drivers

6.1 Overview

GSAOI will be the workhorse instrument for Gemini's MCAO system. The key science drivers for GSAOI were identified at a Gemini community workshop at Santa Cruz in October 2000. These were detailed in the Multi-Conjugate Adaptive Optics (MCAO) Preliminary Design Review (PDR) documentation. The science cases that have been elaborated include:

- Low mass stellar and substellar mass functions in young star-forming regions such as the Orion Nebula cluster.
- Stellar population variations in star-forming regions such as Ophiuchus, Corona Australis, and Chamaeleon.
- Open cluster mass functions to the bottom of the H-burning sequence and the end of the white dwarf cooling sequence to provide independent age determinations.
- Mass functions in nearby globular clusters over a range of metallicities.
- Stellar populations of super-star cluster analogs in the Galaxy and Magellanic Clouds such as NGC 3603 and 30 Doradus.

- SN1a zero point calibration via red giant branch tip star distances to E/S0 galaxies.
- Stellar populations in starburst regions of nearby galaxies.
- Evolution of dwarf irregular versus elliptical galaxies in different environments.
- Early chemical histories of nearby galaxy spheroids.
- Intergalactic stars in nearby galaxy clusters.
- Color distributions among extragalactic globular clusters.
- Spatially resolved spectral energy distributions of high redshift field galaxies.
- Evolution of galaxies in clusters.

It is of key importance to determine whether these science cases can be achieved with the proposed GSAOI instrument and, if not, what more restricted observations are possible. Both limiting sensitivity and guide star availability must be considered in making this assessment.

We add the following science cases to the above list. These projects are of prime interest to GSAOI science team members:

- Missing mass in Magellanic Cloud planetary nebulae.
- Proper motions of Local Group galaxies.
- Stellar populations in dwarf galaxies.
- Measuring H_0 out to 60 Mpc using red supergiants.
- Measuring the bulk motion of galaxies to $cz < 6000 \text{ km s}^{-1}$ with surface brightness fluctuations.
- The formation of the disks of disk galaxies.
- Exploring dark energy via high redshift supernovae.

For each of these cases we now describe the science goal, and then ask the following questions:

- Is the science goal achievable within the sensitivity limits of the proposed instrument?
- Are MCAO guide stars available?
- Does the observation place special requirements on the instrument design?

6.2 The Orion Nebula - A Detailed Study of a Nearby Massive Star-Forming Region

6.2.1 Science Goal

This project was proposed in the MCAO Science Case (RPT-AO-G0107). Deep imaging at J , H , and K is required to identify all stellar objects, brown dwarfs, and planetary mass objects in the central region of the Orion Nebula Cluster down to ~ 1 Jupiter mass. This is required to establish the initial mass function (IMF) in a region of intense massive star formation. A detailed knowledge of the stellar and substellar IMF is fundamental to understanding fragmentation processes in molecular clouds, determining the nature of starburst galaxies, and describing the chemical evolution of the Universe.

The potential for high quality astrometry with MCAO provides a new means of identifying contaminating foreground stars. The Orion Nebula Cluster proper motion is predominantly along the line of sight, so large transverse motions may indicate contaminating sources (0.5 mas yr^{-1} for a transverse velocity of 1 km s^{-1} at the distance of the Orion Nebula). Background stars remain a problem and in fact Lucas et al. (2001) have shown that some $J = 17-18$ mag background stars are seen through the molecular cloud. This problem will increase towards $J = 23$ mag, so the interpretation of color-magnitude diagrams obtained towards Orion will critically depend on assigning accurate membership probabilities.

Accurate membership probabilities can be assigned even for a system with low proper motion like Orion to $H \sim 21.6$ mag over a 2 yr period ($250 \mu\text{as}$ in 4 hr per epoch; c.f. §5.2.8). This corresponds to masses down to $\sim 3-5 M_J$, and represents a significant improvement in the robust assignment of cluster membership over what is currently possible through spectroscopy at the $H \sim 17-18$ mag level. Proper motion information will permit a very robust determination of the Orion Nebula Cluster mass function down to well below the $\sim 10 M_J$ deuterium-burning limit. This mass range overlaps with mass function measurements for extra-solar planets already being obtained from radial velocity work.

6.2.2 Sensitivity Limit

Photometry to $J \sim 26$ mag and H and $K \sim 25$ mag over a 6×6 arcmin field was originally proposed in order to reach $1 M_J$ objects in the Orion Nebula Cluster. The revised limiting magnitude ($H \sim 24.1$, 10:1 in 1 hr) is more restrictive. However, it will still be possible to detect $2 M_J$ objects with ages of $\sim 2 \times 10^6$ yr in the cluster in 4 hr exposures and to confidently assign membership probabilities to 3-5 M_J objects. This can be seen from Figure 5 where H magnitudes based on the models of Baraffe et al. (2002) are plotted for planets and brown dwarfs of different masses and ages of 1 Myr and 5 Myr.

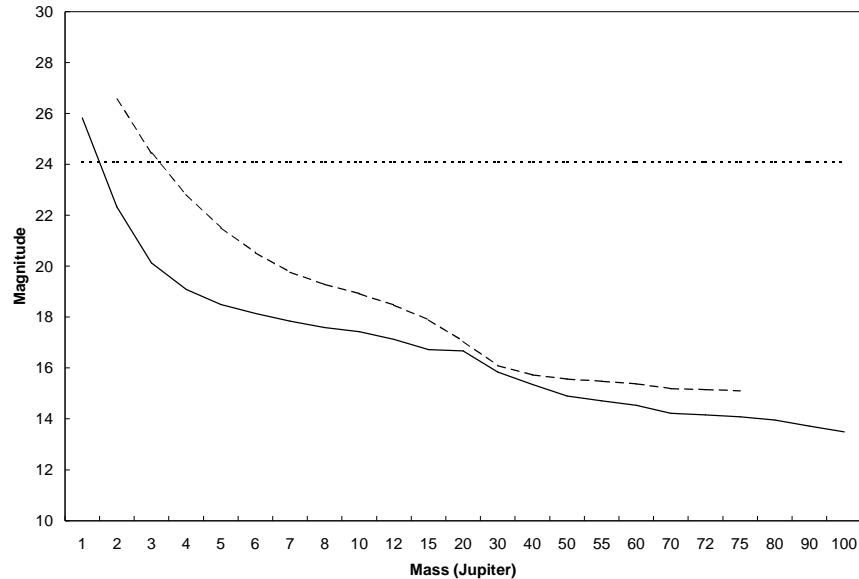


Figure 5: H magnitudes of 1 Myr old (solid curve) and 5 Myr old (dashed curve) planets and brown dwarfs of different masses from Baraffe et al. (2002). The horizontal line corresponds to the 10:1 in 1 hr limit.

6.2.3 Guide Star Availability

There is no difficulty finding suitable guide stars in the center of the Orion Nebula Cluster, as shown in Figure 6. This figure shows DSS, 2MASS, WFPC2, and NICMOS images centered on θ^1 C Ori (the DSS image is saturated by nebula emission). The fields of the four GSAOI detectors are overlaid, along with the outline of the $2'$ diameter MCAO field and the track of the five MCAO LGSs. Three MCAO NGs are marked by triangles. A small circle marks the ODGW star.

The bright nebular background and the bright Trapezium stars limit the sensitivity for detecting faint point sources in the central region. Figure 7 shows a region $3'$ east of θ^1 C Ori. There are no WFPC2 or NICMOS images of this field and the DSS image remains saturated, so no USNO stars are cataloged. The 2MASS near-infrared image suggests that suitable guide stars exist. However, other material will have to be consulted to confirm these selections.

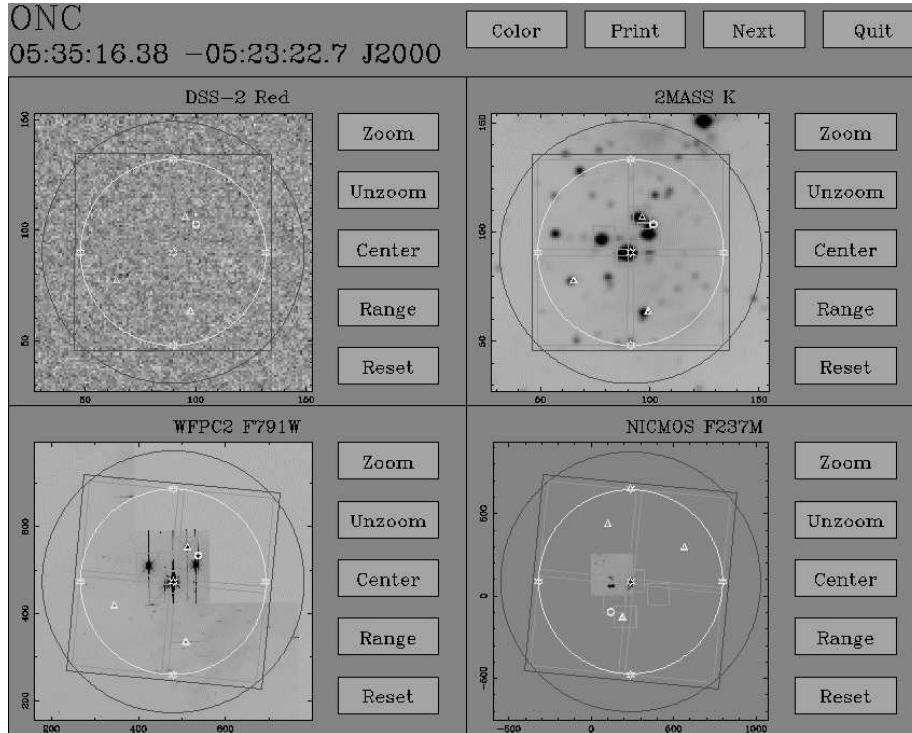


Figure 6: DSS, 2MASS, WFPC2, and NICMOS images of the Orion Nebula Cluster central region. Small squares mark USNO catalog stars. The four GSAOI detectors and the GSAOI field mask are indicated by squares. The large outer circle delimits the MCAO field. Stars mark the five LGSs. Small triangles mark the three NGSs. A small circle marks the ODGW guide star.

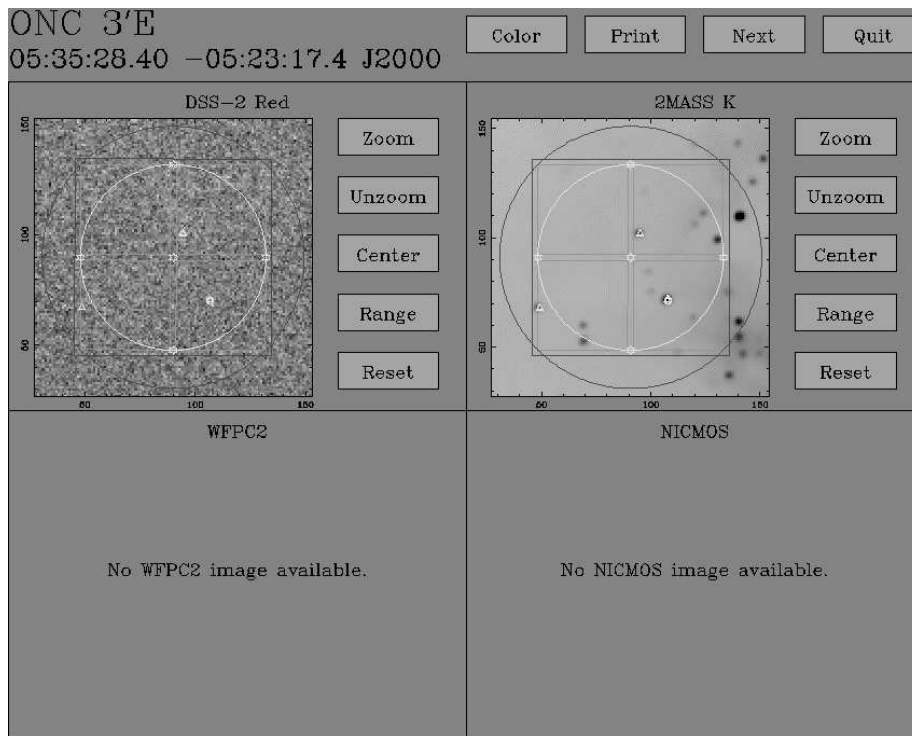


Figure 7: DSS and 2MASS images of a region 3' east of the Orion Nebula Cluster.

6.2.4 *Special Requirements*

The main requirement of this project is to detect faint unresolved objects in the vicinities of multiple bright stars. Low ghost image intensities and low scattered light levels in the imager will be essential.

Long-term high astrometric precision is also essential. The critical issue is whether the astrometric distortion is repeatable at a level significantly below the targeted precision of $\sim 250 \mu\text{as}$ per epoch, for likely changes of the instrument due to flexure and temperature variations. Astrometric distortion residuals of $\sim 50 \mu\text{as}$ per epoch may be required to achieve this.

A simple and straightforward way to calibrate distortion is by imaging a matrix mask at the first telescope focal plane in the MCAO system. Failing that, an acceptable result might be achieved by imaging the 5×5 grid of the MCAO NGS source simulator.

6.3 *Young Stellar Super-Clusters*

6.3.1 *Science Goal*

This project was proposed in the MCAO Science Case (RPT-AO-G0107). It requires deep *J*, *H*, and *K* imaging of Galactic and Magellanic Cloud analogs of the super star clusters identified in starburst galaxies. Super star clusters dominate the star formation in starburst galaxies, and have almost certainly been involved in the star formation history of the Galaxy. Understanding the stellar populations in these massive star-forming regions, and in particular the interplay between high- and low-mass star formation, is a key goal of this project. Mass functions ranging from the massive O-type stars to objects below the hydrogen-burning limit will be studied in nearby young super star clusters such as NGC 3603 in the Galaxy and 30 Dor in the Large Magellanic Cloud. Measurements in narrow-band filters (such as CO and Br γ) will give information on the stellar populations.

6.3.2 *Sensitivity Limit*

NGC 3603 has been measured in $0.4''$ seeing down to $J \sim 21$ mag with ISAAC on the VLT (Brandl et al. 1999). These observations sampled down to masses of $\sim 0.1 M_{\text{Sun}}$ ($\sim 100 M_J$), assuming an age of ~ 1 Myr. Extending this a further 3 mag to the estimated GSAOI *J* limit (~ 24.1 mag 10:1 in 1 hr), or below, will reach substellar objects with masses $< 13 M_J$.

Images of similar depth in the 30 Dor region will reach pre-main sequence stars with masses of a few $\times 0.1 M_{\text{Sun}}$ assuming an age of ~ 1 Myr.

6.3.3 *Guide Star Availability*

NGC 3603 fits easily within the GSAOI field-of-view (Figure 8). There appears to be an abundance of MCAO NGSs, although the lack of USNO catalog stars leaves their brightness uncertain. The 2MASS image shows many potential ODGW guide stars.

The region of the 30 Dor cluster is shown in Figure 9. There appears to be no problem identifying suitable guide stars. However, their brightness cannot be determined from the USNO catalog because the DSS images are saturated.

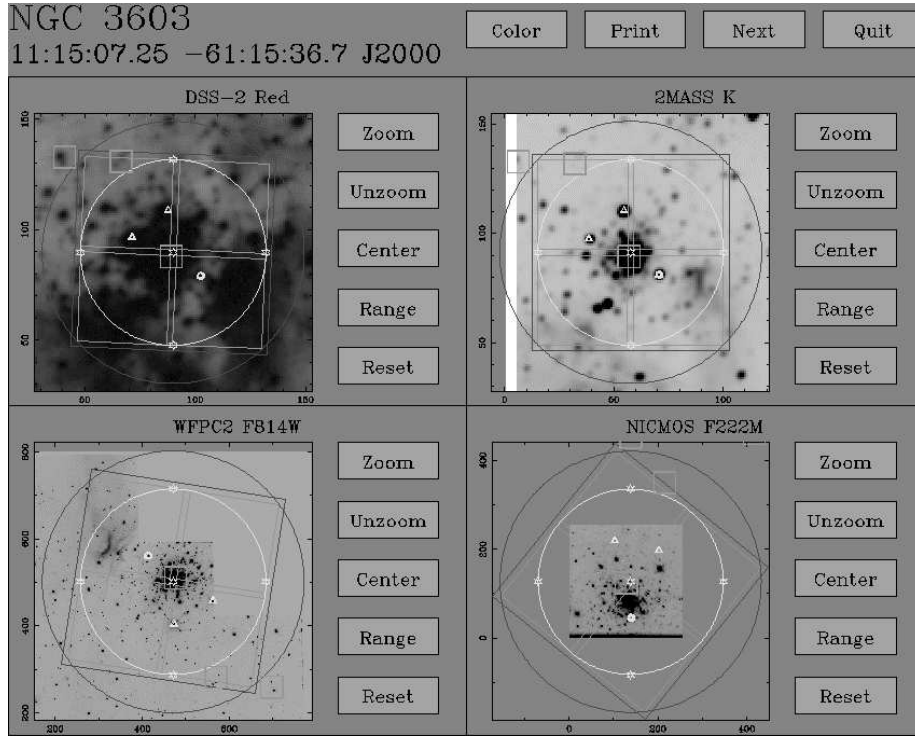


Figure 8: DSS, WFPC2, and NICMOS images of the NGC 3603 star cluster.

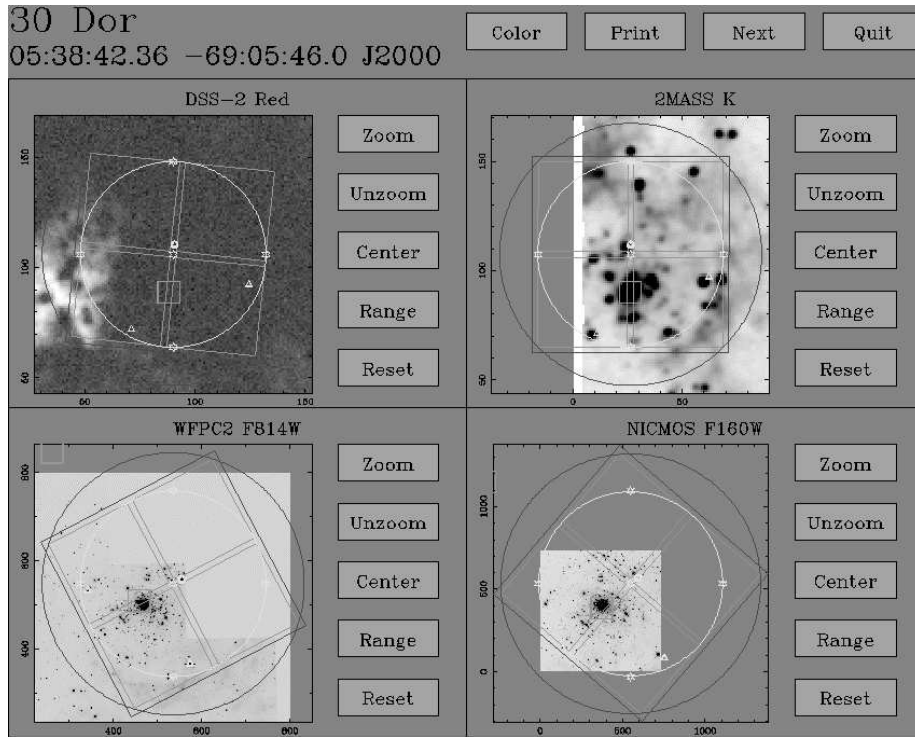


Figure 9: DSS, 2MASS, WFPC2, and NICMOS images of the 30 Dor star cluster.

6.3.4 Special Requirements

The main requirements for this project are high Strehl ratio to reduce crowding, a stable and uniform point spread function (PSF) over the field to permit accurate photometry, and low ghost image intensity to permit high dynamic range measurements in the vicinities of bright stars. A large field-of-view is required, but also good sampling of the PSF at all wavelengths.

6.4 White Dwarf Cooling Ages in Galactic Open Clusters

6.4.1 Science Goal

This project was proposed in the MCAO Science Case (RPT-AO-G0107). The goal is to detect the termination of the white dwarf cooling sequence in nearby open star clusters, and hence derive cluster ages that are independent of the normal main sequence turnoff method. The cooling sequence ends at intrinsically faint magnitudes even for young clusters and contamination by stellar and extragalactic interlopers has always been a concern. The potential for accurate proper motion measurements with GSAOI offers a means of overcoming this difficulty. Proper motion measurements will be especially useful for distinguishing white dwarfs from distant star-forming blue galaxies.

A large area must be mosaiced in order to ensure that the cluster white dwarf luminosity function is adequately sampled.

6.4.2 Sensitivity Limit

Six nearby open clusters spanning a range of ages were identified in the MCAO Science Case; NGC 6405, NGC 2516, NGC 3532, NGC 3680, NGC 6253, and Coll 261. The white dwarf sequence termination has been detected in the 570 Myr old open cluster NGC 2099 at $M_V = 11.95 \pm 0.3$ mag (Kalirai et al. 2001), as expected from its main sequence turnoff age and white dwarf cooling models. This suggests that the white dwarf termination should be detectable with GSAOI in the first four of the clusters listed, with the termination at $H \sim 23.4$ mag in the oldest of these, NGC 3680. Termination magnitudes in the older clusters, NGC 6253 and Coll 261, are expected to be significantly below the GSAOI sensitivity limit of $H \sim 24.1$ mag (10:1 in 1 hr).

6.4.3 Guide Star Availability

There appears to be no shortage of guide stars towards these Galactic open clusters. The extreme central region of NGC 6405 is shown in Figure 10.

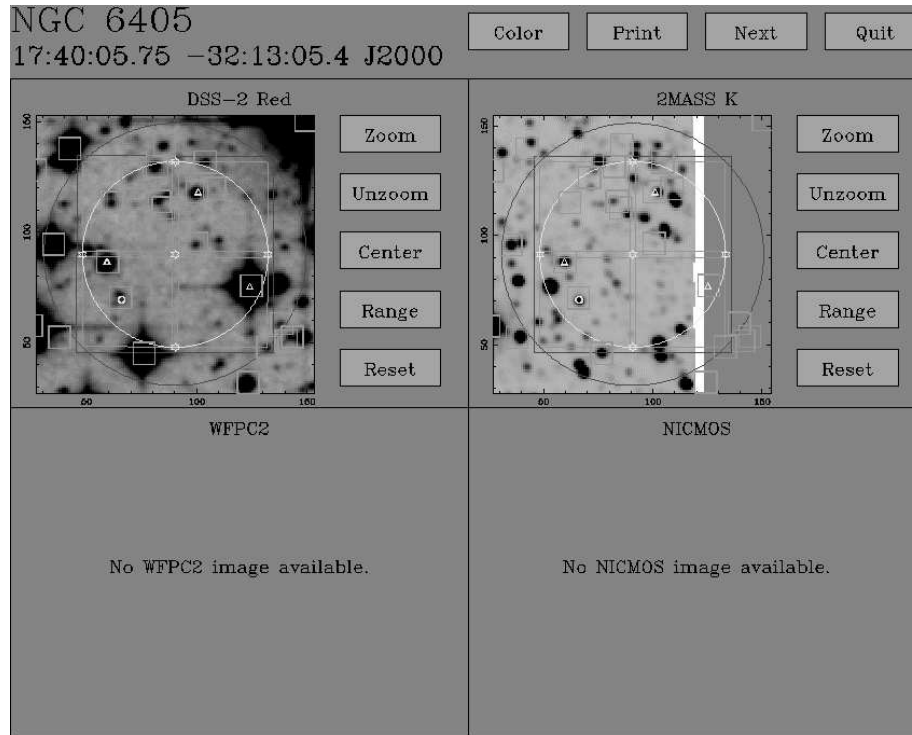


Figure 10: DSS and 2MASS images of the extreme central region of the open cluster NGC 6405.

6.4.4 Special Requirements

The main requirement for this project is high astrometric precision to identify open cluster members. The maximum possible field size with good PSF sampling is desirable to increase the number of detected stars. Stars are expected over a range of ~ 10 mag so high dynamic range is also desirable.

6.5 Globular Cluster Mass Functions Over a Range of Metallicities

6.5.1 Science Goal

This project was proposed in the MCAO Science Case (RPT-AO-G0107). It aims to probe the main sequence mass function and substellar limit in old metal-poor Galactic globular clusters. The mass limit of stars at the bottom of the hydrogen-burning main sequence is predicted to be metallicity dependent: this prediction will be tested. Deep *JHK* images reaching the end of the population-II main sequence are required for several globular clusters. Measurements of proper motions will be used to identify cluster members and remove field stars.

6.5.2 Sensitivity Limit

The MCAO Science Case lists five southern globular clusters that are suitable for this project; NGC 6553, NGC 104, NGC 6121, NGC 6752, and NGC 6397. The bottom of the hydrogen-burning main sequence in globular clusters should occur at $M_J \sim 13$ mag and $M_K \sim 11$ mag. Sixteen fields and at least two filters are required per cluster, so exposure times are effectively limited to ~ 1 hr. Given the expected GSAOI sensitivities ($J \sim 24.1$ mag and $K' \sim 23.9$ mag 10:1 in 1 hr), it is likely that the bottom of the main sequence will be detectable in only NGC 6121 and NGC 6397, and detection at *J* will be difficult even in these clusters ($J \sim 24.7$ mag and $K \sim 22.7$ mag for NGC 6121; $J \sim 24.8$ mag and $K \sim 22.8$ mag for NGC 6397). The bottom of the main sequence is expected to be at $J > 26.0$ mag and $K > 24.0$ mag in the other clusters.

6.5.3 Guide Star Availability

There is no difficulty identifying guide stars, at least in the central regions of NGC 6121 and NGC 6397. The core of NGC 6121 is shown in Figure 11.

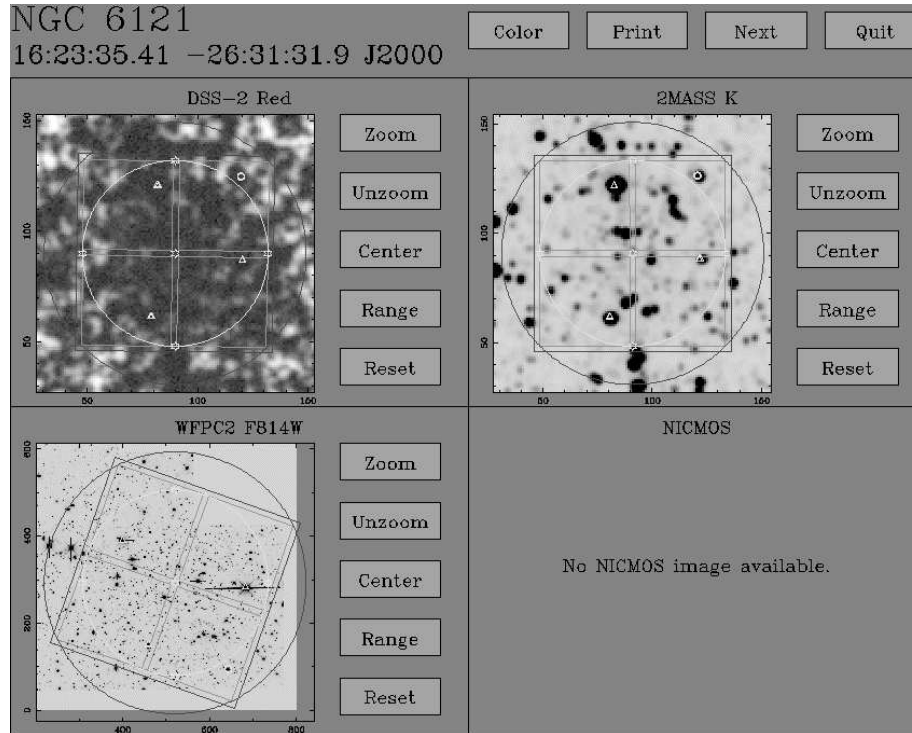


Figure 11: DSS, 2MASS, and WFPC2 imagers of the core of the globular cluster NGC 6121.

6.5.4 Special Requirements

A uniform PSF across the GSAOI field-of-view is required to perform accurate photometry at faint levels.

6.6 Missing Mass in Magellanic Cloud Planetary Nebulae

6.6.1 Science Goal

Despite vast increase in our understanding of the evolutionary nature of planetary nebulae (PNe) during the last three decades, a central question remains: *where is the missing mass?* Theoretical evolutionary tracks predict that all stars with masses in the range $1.4\text{--}8 M_{\text{Sun}}$ should become PNe. According to the models, much of the mass of these stars is lost during a series of thermal pulses in the asymptotic giant branch (AGB) phase of evolution. Observations reveal that the central star mass is close to $0.6 M_{\text{Sun}}$, except for a few Peimbert Type I nebulae (e.g., NGC 6302 with $0.8 M_{\text{Sun}}$, or a handful of objects in the LMC). However, the ionized nebular mass of the PN is typically of order $0.1 M_{\text{Sun}}$, and the derived mass is found to depend very strongly on the radius of the nebula. Clearly, much of the mass of the planetary nebula shell must remain un-ionized, and much of it may be in molecular form. This molecular gas has been mapped in the 110.2 GHz (1-0) transition of ^{12}CO in a number of nearby PNe. These observations confirm the much greater extent of the nebula in molecular gas. In the infrared, the nebula can be mapped in the $2.122 \mu\text{m}$ 1-0 S(1) and $2.248 \mu\text{m}$ 2-1 S(1) lines of molecular hydrogen, which in most objects seem to be fluorescently excited by UV radiation from the central star. Generally speaking, the size of the observed nebula is larger, and the estimated molecular hydrogen masses much greater, than the ionized gas component. The nebula of NGC 7027 (Dayal et al. 2000) is a splendid example of this.

For Galactic objects, accurate mass inventories are bedeviled by uncertainties in the PN distance scale, which can only be resolved by the study of a population of PN at a known distance and having low field reddening. The Magellanic Cloud PNe are ideal for this. At optical wavelengths, the Hubble Space Telescope (HST) has been used to systematically investigate the morphologies and ionization of the ionized component. These data typically have a spatial resolution of a little better than $0.1''$, which corresponds to a linear resolution of ~ 0.02 pc at the distance of the LMC. This is quite sufficient to reveal the internal morphology, given that the typical diameter of a PNe is about 0.1 pc and some objects are as large as 1.0 pc across including the faint outer structure.

With its superb spatial resolution, the GSAOI instrument will be ideally suited to perform a systematic study of both the PNe and the proto-planetary nebulae in the Magellanic Clouds at a spatial resolution that matches the observations that have been made by HST of the ionized gas components. The quality of the images that could be obtained would be comparable with the NICMOS images that HST has obtained of PNe towards the Galactic center. Not only can the extent and distribution of the molecular hydrogen be determined, but the PNe can also be mapped in the [Fe II] $1.644 \mu\text{m}$ line, which in some PNe reaches an intensity in excess of $2 \times 10^{-14} \text{ erg cm}^{-2} \text{ s}^{-1} \text{ arcsec}^{-1}$ (Welch et al. 1999) and which traces the positions of shocks driven into the molecular shell by the high pressure of the ionized zone and fast winds that have shaped the PNe morphology.

For the Magellanic Cloud PNe, these data will enable us to derive quantitative data that cast direct light on the evolution of PNe and on their AGB precursors. The positions of the central stars on the Hertzsprung-Russell diagram are known, we can distinguish between H-burning and He-burning stars, and the dynamical ages of the nebulae can be determined for these PNe.

6.6.2 Sensitivity Limit

The average intensity of [Fe II] $1.644 \mu\text{m}$ emission in the outer parts of the Galactic planetary nebula Hubble 12 is $\sim 8 \times 10^{-15} \text{ erg s}^{-1} \text{ cm}^{-2} \text{ arcsec}^{-2}$ (Welch et al. 1999). The sensitivity limit for GSAOI in the [Fe II] $1.644 \mu\text{m}$ filter is expected to be $\sim 4 \times 10^{-15} \text{ erg s}^{-1} \text{ cm}^{-2} \text{ arcsec}^{-2}$ (10:1 per resolution element in 1 hr). This is comfortably below the expected average intensity, so it will be possible to confidently detect any low surface brightness structure that is present.

6.6.3 Guide Star Availability

Twenty-six LMC PNe (Vassiliadis et al. 1998 and references therein) with HST data have been searched for suitable MCAO guide stars. Acceptable guide stars are probably available for all of these targets. We illustrate this with the example of LMC-SMP 2 in Figure 12. Nevertheless, it is apparent that the ability to dither the image to achieve accurate sky subtraction is often restricted by the need to have suitable guide stars at every dither position.

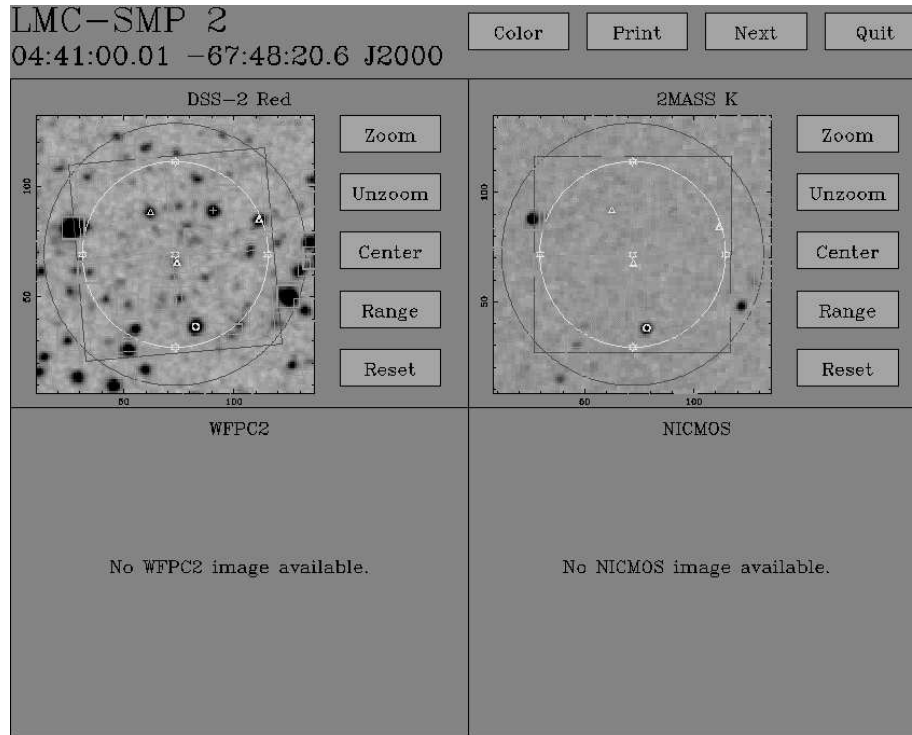


Figure 12: DSS and 2MASS images of the LMC planetary nebula LMC-SMP 2. A small cross identifies the target.

6.6.4 Special Requirements

The Large and Small Magellanic Clouds have heliocentric Doppler shifts of $+260$ and $+150$ km s^{-1} , respectively. The "zero redshift" narrow band emission line filters should be sufficiently wide (or have appropriately shifted central wavelengths) to ensure that emission lines from both Galactic and Magellanic Cloud objects are passed with good transmission.

A uniform PSF over the GSAOI field will permit deconvolution algorithms to be used to further improve spatial resolution.

6.7 Proper Motions of Local Group Galaxies

6.7.1 Science Goal

The accretion of satellites (Searle & Zinn 1978) has become recognized as being of fundamental importance to the formation and evolution of the Milky Way halo. This model was initially proposed because differences in the globular cluster populations in the inner and outer halo suggested the existence of an age spread (Zinn 1993; van den Bergh 1993). Studies in recent years have provided several lines of evidence to support the importance of the accretion scenario, including:

- Numerous examples of kinematic substructures along independent lines of sight that suggest the halo is threaded with "streams" of stars (e.g., Arnold & Gilmore 1992; Côté et al. 1993; Majewski et al. 1994).
- The discovery of the "smoking gun" of the Sagittarius dwarf spheroidal galaxy that has been "caught in the act" of being disrupted by the Milky Way (Ibata et al. 1994).

However, the properties of a typical accretor remain unclear.

It has been long suggested that the Milky Way satellites define a plane about the Galactic center (Kunkel & Demers 1976; Lynden-Bell 1976). More recently, two separate planes have been proposed (Majewski et al.

1994; Lynden-Bell & Lynden-Bell 1995). If such "mega-streams" are associated with a single accretion event, a typical accretor would have a mass comparable to the Magellanic Clouds. Alternatively, accretion events may have involved only single dwarf spheroidal-like satellites, implying a "maximally chaotic" outer halo in which a typical stream has a mass of $< 10^8 M_{\text{Sun}}$, and the "mega-streams" are not dynamically significant. The distinction between high- and low-mass accretors is important. The latter (10^7 - $10^8 M_{\text{Sun}}$) will produce kinematically distinct streams that survive for long times in the halo, while negligibly heating the Galactic thin disk. The accretion of a massive satellite, however, would produce a kinematically indistinct cloud of stars and heat the disk to much larger scale heights than we see today.

Space velocities will allow us to determine how well mixed the outer halo really is, and test directly for the existence of the "mega-streams". Proper motions are vital for this, as they alone distinguish between chance alignments and true streams. Precise proper motions for the Galaxy's satellites are essential if we are to distinguish between these models.

Such data are also of fundamental importance to the determination of the gravitational potential of the Galaxy at large galactocentric radii, and to the measurement of the total mass of our Galaxy.

GSAOI offers the prospect of the precise measurement for many southern hemisphere satellite galaxies such as Fornax, Sculptor, Carina, Sextans, Phoenix, and others. Dedicated surveys have revealed the presence of unresolved quasars behind many of these target galaxies (Tinney et al. 1997; Tinney 1999), and similar surveys of the remaining targets will be straightforward to carry out. At the magnitudes of interest, both quasars *and* suitable giants in the galaxies for use as a "galaxy" reference frame are available (the technique is to measure the quasar's reflex motion relative to a frame of galaxy giants). At precisions of $\sim 180 \mu\text{s}$ per epoch over 5 years, 1σ precisions for proper motion measurement of $\sim 40 \mu\text{as yr}^{-1}$ become feasible, making the proper motions of all these galaxies detectable in a program totaling ~ 200 - 300 hr over 5 years.

6.7.2 Sensitivity Limit

The Sculptor, Sextans, Carina, Fornax, Phoenix dwarf spheroidal galaxies have distance moduli of 19.5, 19.7, 20.0, 20.7, and 23.2, respectively. The red giant branch tip occurs at $M_K \sim -6.5$ mag, so these stars will be detected at $K \sim 13.0, 13.2, 13.5, 14.2,$ and 16.7 mag, respectively. Red giant branch stars will be easily measured with GSAOI. Integration times will be set by the required astrometric precision, rather than photometric precision. Some red giant branch tip stars are so bright that they will saturate the detector in the minimum integration time of 5 s. These stars should be avoided.

6.7.3 Guide Star Availability

Guide star availability will depend on the positions of background quasars projected on the foreground galaxy. This is uncertain at present.

6.7.4 Special Requirements

Long-term high astrometric precision is essential.

6.8 Stellar Populations in Dwarf Galaxies

6.8.1 Science Goal

It is probably no exaggeration to claim that the most important outstanding question in the study of the formation and evolution of dwarf galaxies is the origin of the remarkable diversity of star formation histories observed among the dwarf Ellipticals (a class that includes the so-called dwarf Spheroidals) of the Local Group. Prior to the first hints of a discrepancy in the early 1980s, the paradigm that dEs galaxies consist entirely of old stars was universally accepted, and amongst those unfamiliar with developments in the field, this view is still surprisingly prevalent. Yet it is now abundantly clear that the simple picture of dEs as consisting of entirely old (age > 10 Gyr) stars is no longer valid. For example, among the Milky

Way's dE companions we see systems with dominant old populations, systems with minor intermediate-age (age ~ 2 to 10 Gyr) components, and systems where the intermediate-age component dominates the old stars. Even in these latter systems there is further variety; in Carina the on-going star formation occurred in a number of discrete episodes while in Fornax it was approximately continuous. This variety of star formation histories is not restricted to the Galaxy's companions. Recent observations with HST/WFPC2 have shown that M31's dEs have also had extended epochs of star formation.

Despite the large amount of observational data available for Local Group dEs, there is currently no explanation for the diversity of star formation histories, only hints. For example, among the Galaxy's companions there is a tendency for the systems with stronger intermediate-age components to lie at larger Galactocentric distances. This also appears to be the case for M31's companions where, at least among the lower luminosity dE companions, it is the more distant system And II that has a definite intermediate-age population; systems closer to M31 lack such stars. These results suggest that proximity to a "parent galaxy" influences the evolution of dwarf galaxies. Indeed, recent theoretical simulations have shown how a dwarf irregular on an initial "plunging" orbit in the Milky Way halo can be converted into a dE satellite. At the same time it is notable that, with one exception, all the isolated dwarfs in the Local Group are not dEs; they show either recent or on-going star formation. The one local exception to this hypothesis that "parent galaxies" nurture initial gas-rich dwarf companions into dE galaxies, is the isolated dE Tucana. Despite its lack of association with any large galaxy, it nevertheless possesses a dominant old stellar population and there are no signs of any intermediate-age component. The existence of this system demonstrates that proximity to a large galaxy cannot be the only factor governing the evolution of dwarf galaxies.

To make progress in understanding the processes that govern dwarf galaxy evolution, we need to study systems beyond the Local Group. Such studies can be targeted at dEs that occupy a variety of environments, thereby allowing us to more readily distinguish between intrinsic properties and "parent galaxy" influence. In particular, we need to target a sizeable fraction of the dEs within our "Local Volume", the sphere of radius ~ 10 Mpc centered on the Local Group, seeking to establish what fraction of these systems show intermediate-age populations. This volume includes the relatively loose Sculptor Group, the more compact Cen A group, and a variety of other galaxy aggregations such as the loose association of galaxies that contain the Circinus galaxy at a distance of 6-7 Mpc. The observational signature of an intermediate-age population is the presence of upper-AGB stars, i.e., stars with sufficient mass to evolve on the AGB to luminosities above that of the red giant branch tip. For such stars there is a good correlation between the luminosity of the brightest upper-AGB star and the age of the intermediate-age component. The observations are best done at near-infrared wavelengths since these pass bands cover the wavelengths where the majority of the flux is emitted. Bolometric corrections are therefore small and well defined and the amplitude of variability is much reduced relative to the optical. Single epoch J and K band measurements then suffice for a determination of the bolometric magnitudes (two pass bands are required as the bolometric correction to the K magnitude is a function of $J-K$ color). Although current near-infrared imagers can reach upper-AGB stars in the nearer of the dEs within the Local Volume using relatively long integration times, given the likelihood of a diversity of star formation histories, a sizeable sample of dwarfs in a variety of environments needs to be studied if underlying trends are to be revealed. GSAOI is the ideal instrument with which to carry out this program.

6.8.2 Sensitivity Limit

An 8-10 Gyr old upper-AGB star, the upper limit to what we might call an intermediate-age population, has a bolometric magnitude $M_{\text{Bol}} \sim -4.1$ mag and $M_K \sim -6.8$ mag with $J-K \sim 1.2$. We need to measure the bolometric magnitude to a precision of $\sim \pm 0.2$ mag, including both photometric and distance modulus uncertainties. This can be achieved if both the J and K magnitudes are measured to a signal-to-noise ratio of ~ 10 . The expected GSAOI sensitivities are such that the upper-AGB component can be measured for any dE within the 10 Mpc sphere of the Local Volume in ~ 1 hr of on-source integration at K and 5 hr of integration at J . This is sufficient sensitivity to allow targeting of a well-defined sample of dEs covering a range of both intrinsic properties (surface brightness, total magnitude, length scale, etc.) and environmental parameters (distance from potential parent galaxy, parent galaxy type, local galaxy density, orbit timescales/crossing times, etc.).

6.8.3 Guide Star Availability

There are sufficient candidate dE galaxies within the Local Volume that restricting the sample to only those systems with appropriate guide stars is not likely to be a severe requirement. The relatively small size of the targets also allows some flexibility in the positioning, increasing the probability of acquiring a suitable set of guide stars. An example is shown in §8.1.

6.8.4 Special Requirements

The program described here is essentially a routine application of the GSAOI and therefore does not impose any special requirements on the instrument other than a uniform PSF across the field to permit accurate photometry.

6.9 Calibration of the Supernovae Ia Zeropoint

6.9.1 Science Goal

This project was proposed in the MCAO Science Case (RPT-AO-G0107). The goal is to measure red giant branch tip distances to E/S0 galaxies containing supernovae (SNe) Ia. These SNe Ia can then be used to tighten the SNe Ia distance scale calibration. The red giant branch tip occurs at $M_J \sim -5.3$ mag and $M_K \sim -6.5$ mag, but it is necessary to reach somewhat below the tip in order to make a confident detection. The MCAO Science Case lists seven E/S0 galaxies with well measured SNe Ia; NGC 1316, NGC 5128, NGC 4374, NGC 1380, NGC 4526, NGC 5253, and NGC 5003.

6.9.2 Sensitivity Limit

The expected GSAOI sensitivity ($J \sim 24.1$ mag and $K_s \sim 23.8$ mag 10:1 in 1 hr) is such that the red giant branch tip is likely to be detectable only in NGC 5128 and NGC 5253 at $J \sim 22.5$ mag and $K_s \sim 21.3$ mag and $J \sim 22.9$ mag and $K_s \sim 21.7$ mag, respectively. The red giant branch tip has already been detected in NGC 5128 (Soria et al. 1996). The red giant branch tip occurs at $J \sim 25.1$ mag and $K \sim 23.9$ mag in NGC 5005 and at $J > 25.7$ mag and $K > 24.5$ mag in the other five galaxies. It is therefore likely that GSAOI will permit only a minor improvement in the SNe Ia distance scale calibration.

6.9.3 Guide Star Availability

Suitable guide stars appear to be available in a field ~ 1.5 arcmin SE of the nucleus of NGC 5253 (Figure 13). The MCAO NGSs have $R \sim 15.8$, 18.0, and 18.1 mag in the USNO catalog. Concerns about the calibration of the USNO catalog in the southern hemisphere dictate caution in choosing the two fainter stars. The $R \sim 15.8$ mag star is chosen as the ODGW guide star, although this object appears faint in the 2MASS K band image.

Guide stars are available in a field 4' south of NGC 5128.

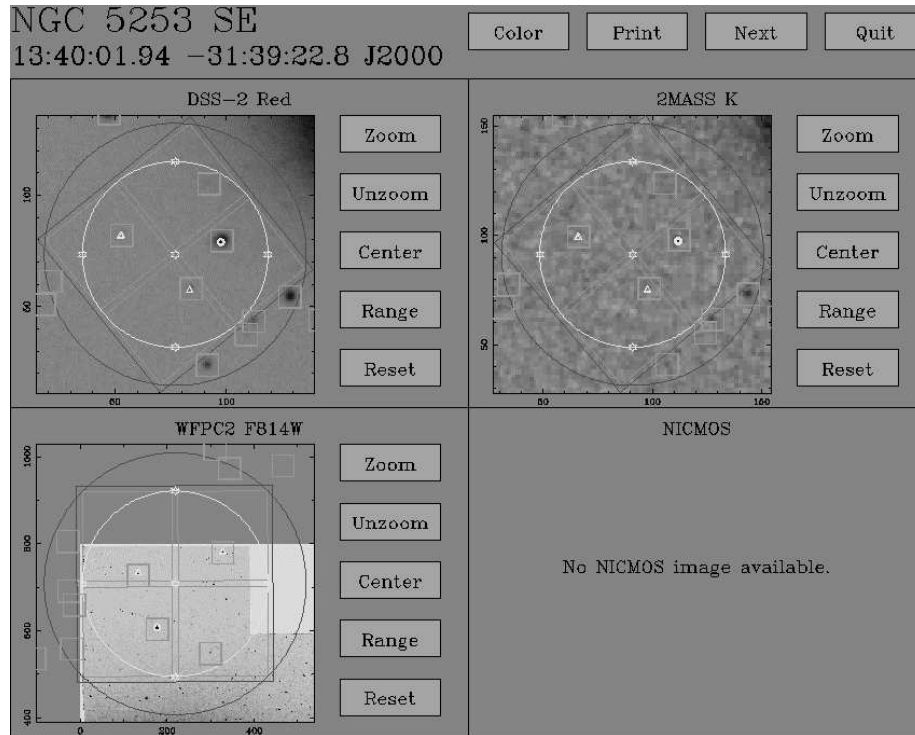


Figure 13: DSS and WFPC2 images of a field ~ 1.5 arcmin SE of NGC 5253.

6.9.4 Special Requirements

The project is essentially a routine application of the GSAOI and therefore does not impose any special requirements on the instrument other than a uniform PSF across the field to permit accurate photometry.

6.10 Intracluster Stars in Nearby Galaxy Clusters

6.10.1 Science Goal

This project was proposed in the MCAO Science Case (RPT-AO-G0107). Faint intracluster light is seen in some of the more distant galaxy clusters. It is currently believed to come from stars stripped from galaxies by the harassment process (fast encounters of galaxies leading to impulsive heating and then stripping by the tidal field of the cluster). This belief needs to be more firmly established.

In the nearer clusters, like Virgo and Fornax, observations of diffuse light are very difficult. Individual stars are much more useful tracers of the stellar intracluster medium (ICM) in nearby clusters; intracluster planetary nebulae have already been detected in the Virgo and Fornax clusters.

Galaxies of intermediate mass are believed on theoretical grounds to be the ones most affected by harassment. They can be transformed into loosely bound dwarfs, with much of their stellar mass lost into the ICM. The harassment process would produce a stellar ICM with substantial substructure in space and velocity. This can be tested directly, and some progress has been made in this direction using the planetary nebulae.

Red giants are much more abundant than planetary nebulae, and provide ideal probes of the ICM. In principle, one can use color-magnitude diagrams (CMDs) of the upper giant branch of the intracluster stellar population to derive the surface density distribution and the metallicity of the stellar ICM. This would allow us to quantify the spatial substructure of the ICM; also, using the metallicity-luminosity

relation for galaxies, it would give useful observational constraints on the kinds of galaxies that have contributed most to the stellar ICM.

The observational goal is then to construct stellar CMDs in many locations of the Virgo and Fornax clusters; these are the nearest significant galaxy clusters, and are both known to contain a stellar ICM.

6.10.2 Sensitivity Limit

Here is the problem. To do anything useful on the stellar ICM, we need a CMD down to at least 1 mag below the tip of the red giant branch. The brightest red giants have $M_J = -5.5$, $M_H = -6.2$, and $M_K = -6.5$ mag. The distance modulus of the Virgo and Fornax clusters is ~ 31.0 . So we need images with a signal-to-noise ratio of at least 5 at $J = 26.5$, $H = 25.8$, and $K = 25.5$ mag. This seems well out of reach for the GSAOI. Even with a small aperture of 4×4 pixels, the on-source integration times at J , H , and K are about 21, 6, and 5 hr, respectively.

6.11 Measuring H_0 Out to 60 Mpc Using Red Supergiants

6.11.1 Science Goal

Despite intense efforts using HST over the past decade, there is still fierce debate about the value of the Hubble Constant, although most people now agree that it has a value between 55 and 80 km s⁻¹ Mpc⁻¹. The HST Key Project team has presented the most significant body of work (Freedman et al. 2001). They used Cepheid variables out to 20 Mpc as the calibrating method for a host of secondary distance indicators such as Type Ia supernovae, surface brightness fluctuations, and the Tully Fisher method. However, the small numbers of objects, difficulties in HST CCD calibrations, large extinction corrections, and the difficulty of combining surface brightness fluctuation distances to early-type galaxies with Cepheid distances to late type galaxies have all complicated this work. Luminous red supergiants provide a new method of measuring the Hubble constant that is independent of Cepheid distances. The red supergiant method offers high precision, ease of use, low vulnerability to extinction, and a single method that can be applied to the LMC, SMC, nearby galaxies, and other late-type galaxies out to 60 Mpc with GSAOI.

The brightest red supergiants pulsate with periods of 400 to 900 days and have $M_K \sim -11$ (Wood, Bessell, & Fox 1983). Typical full K band amplitudes are ~ 0.25 mag. These luminous red supergiants lie on a K -log P relation with scatter about the relation of ~ 0.25 mag. The LMC has roughly 20 of these variable red supergiants so that a galaxy of this relatively small size can give a distance modulus accurate to ~ 0.05 mag. Larger spiral galaxies will yield larger numbers of red supergiants and hence a more accurate distance modulus. Imaging in the K band maximizes the contrast between the red supergiants and the galaxy background. Red supergiants will be found by their variability, which distinguishes them from bright star clusters.

The degree of contrast of the red supergiants against the galaxy background is a relevant concern that will be more problematic at larger distances. If a typical background giant star has $M_K \sim -5$ mag, its apparent magnitude at a distance of ~ 60 Mpc is $K \sim 28.9$ mag. There are ~ 83 such giant stars per $0.06'' \times 0.06''$ resolution element in a region with a K band surface brightness of ~ 18.0 mag arcsec⁻². Background fluctuations due solely to statistical variations in the number of these stars will be at the level of $\Delta K \sim \pm 0.1$ mag per resolution element. The addition of a single $M_K = -11$ mag red supergiant to this background will cause a fluctuation of -1.5 mag per resolution element. Consequently, it is very unlikely that surface brightness fluctuations due to variations in the number of background stars will impede measurement of the luminous red supergiants.

6.11.2 Sensitivity Limit

A signal-to-noise ratio of ~ 25 is required to detect variability. The GSAOI K band sensitivity is such that a $M_K \sim -11$ mag red supergiant can be detected with this signal-to-noise ratio at 60, 50, 40, 30, and 20 Mpc in 1.0, 0.5, 0.2, 0.06, and 0.01 hr. Approximately 12 such measurements spread over ~ 2 years at 2-3 month

intervals are required to determine a pulsation period. At least three galaxies are required at each distance, so this project will require a total of ~ 65 hr of on-source integration time to complete.

This program can easily be expanded to increase the number of galaxies surveyed, and improve the precision of Hubble constant measurement and the volume sampled.

6.11.3 Guide Star Availability

There is a multitude of acceptable galaxies at distances < 60 Mpc, so it is convenient to choose only galaxies that have suitable guide stars.

6.11.4 Special Requirements

A uniform PSF is required over the GSAOI field to allow accurate measurement of stars across the entire galaxy.

6.12 Measuring the Bulk Motions of Galaxies to $cz < 6000$ km/s with Surface Brightness Fluctuations

6.12.1 Science Goal

It is widely accepted that the evolution of the large scale structure of the Universe is driven by dark matter. Understanding this dark matter continues to be one of Astronomy's great unsolved problems. Measuring the bulk motions of galaxies allows us to map the overall mass distribution of the Universe in a way that is independent of the luminous matter in galaxies. Each galaxy whose motion is measured, serves as a test particle of the gravitational field around it. With large numbers of accurately measured objects it is possible to reconstruct the mass distribution of material in the Universe. Unfortunately, this has not been easy – since the first results of 15 years ago of the “Great Attractor” (Lynden-Bell et al. 1988), the field has been littered with contradictory results and findings that are still not understood. The heart of the problem has been finding a way to obtain large numbers of accurate distances between $0 < cz < 10,000$ km s⁻¹. GSAOI can make significant progress in this field by measuring *H* band surface brightness fluctuation (SBF) distances to hundreds of galaxies in this range. Already SBF has been used at optical wavelengths to probe motions at $cz < 2000$ km s⁻¹, but this work was hampered by the fact that much of the action happens outside of 2000 km s⁻¹ (Tonry et al. 2000).

H band surface brightness fluctuations (Jensen et al. 2001) provide distances accurate to ~ 0.12 mag, and are limited, in the case of GSAOI, by contamination from globular clusters at $cz > 8000$ km s⁻¹, not by photometric uncertainty. Using observations of ~ 100 SBF galaxies in the direction of the Great Attractor, the location, mass, and extent of the Great Attractor could finally be ascertained by looking at the motion of galaxies on all sides of this object. An additional survey of ~ 500 galaxies at $cz < 6000$ km s⁻¹ across the whole sky would provide a new scale measurement of bulk motions in the current Universe, and provide a measurement of the scales over which dark matter clusters.

6.12.2 Sensitivity Limit

A 0.12 mag *H* band SBF measurement requires reaching $H \sim 23$ mag with a signal to noise ratio of 10. GSAOI can reach this level of sensitivity in ~ 10 min of integration time. This level of integration is appropriate for nearly all the galaxies in the bulk motion sample. In total, we estimate that this program needs ~ 200 hr of integration time to carry out its objectives, although the program could be expanded to any amount of observing time by increasing the sample of galaxies.

6.12.3 Guide Star Availability

There are tens of thousands of acceptable galaxies at $cz < 6000$ km s⁻¹, and therefore it is possible to choose those galaxies that have appropriate guide stars.

6.12.4 *Special Requirements*

A uniform PSF over the GSAOI field is required to accurately measure the surface brightness fluctuations. The large field of GSAOI also would allow multiple galaxies to be imaged simultaneously in those nearby clusters and groups that have appropriate guide stars.

6.13 *The Formation of the Disks of Disk Galaxies*

6.13.1 *Science Goal*

The formation of the disks of disk galaxies remains poorly understood. Cold Dark Matter (CDM) simulations have difficulty in reproducing the observed properties of disks. For example:

- The disks that are formed in the simulations have significantly smaller scale lengths and less angular momentum than real galactic disks.
- Many disk galaxies have only the thin disk component, with no bulge or significant thick disk. This means that they formed in a very quiescent way, with no star formation occurring before the gas disk had settled. Furthermore, since the epoch of disk settling, there cannot have been any significant disturbance by the mergers and interactions that are such a feature of the CDM simulations.

Other important problems include:

- Almost all disk galaxies have an exponential radial surface brightness distribution. The reason for this exponential form is not known; nor is it known when the exponential form is established.
- The exponential disks are typically truncated radially at a radius of about 3 exponential scale lengths. This truncation is an important and probably fundamental indicator of the nature of the galaxy formation process. At this time, the reason for the truncation is not known. Here are some of the many possibilities:
 - The truncation may reflect the maximum angular momentum of baryons in the protogalaxy, or
 - It may be caused by tidal interactions of lumps of dark + baryonic matter early in the hierarchical aggregation process, or
 - It may be the radius where the gas density goes below the critical density for star formation, or
 - It may be associated with the viscous evolution of the star-forming disk (which itself may also lead to the exponential light distribution).

Almost everything that we know about galactic disks comes from disks at low redshift, so little is known about when the fundamental properties of the disks were established. MCAO gives us the opportunity to study the detailed structure of galactic disks at earlier epochs, to a redshift $z = 1$.

The primary goal is to see if the exponential nature of the disks, their characteristic scale lengths and their truncation are already established at $z = 1$. To achieve this goal, we need the high spatial resolution and high near-infrared sensitivity offered by the GSAOI. Observationally, we would aim to study galaxies over a range of redshifts, but at the same rest-frame mean wavelength. We would compare low redshift galaxies observed in the I band with galaxies at $z = 0.5$ in the J band and at $z = 1$ in the H band.

Resolution: For a disk galaxy like the Milky Way, with a scale length of 4 kpc, the expected truncation radius at $z = 1$ in a standard Λ -universe is about 1.8". Such galaxies are very well suited to surface photometry in J and H with GSAOI.

Near-infrared imaging: For low redshift spirals, the large scale structure of the disk depends on wavelength. This is partly due to the star formation history and partly to internal absorption. We therefore need to compare low and higher redshift galaxies with observations at the same rest-frame mean

wavelength. Although one could cover the redshift range $z = 0$ to 1 using observations in B and I , this would be far from ideal; dust and star formation affect the surface photometry much more at shorter wavelengths. It is better to make the low redshift observations in the I band and the higher redshift observations in the near-infrared.

We would propose to survey disk galaxies in the field and in a sample of clusters, at redshifts around $z = 0.5$ (J), $z = 1$ (H) and $z = 1.7$ (K_s).

6.13.2 Sensitivity Limit

The goal is to do surface photometry of our disk galaxies out to a radius of ~ 3.5 scale lengths. We estimate the required integration times, assuming conservatively that the intrinsic (rest-frame) central surface brightness of our galactic disks is independent of redshift and similar to that most commonly seen among normal low redshift disks ($\mu_1 = 19.8$ mag arcsec⁻² or 1.5×10^{-17} erg cm⁻² s⁻¹ Å⁻¹ arcsec⁻²). We also assume that the typical exponential scale length is 4 kpc. Using ellipse-fitting surface photometry, with 6 radial bins extending out to 3.5 scale lengths, and requiring a signal-to-noise ratio of 3 in the outermost bin, we would need an integration time of ~ 10 min at J for the $z = 0.5$ galaxies and 1.2 hr at H for the $z = 1$ galaxies.

For disks of normal rest-frame surface brightness, the observed surface brightness at $z = 1.7$ is too faint for us to do this kind of photometry in the K band. However, if the rest frame surface brightness is 0.5 mag brighter than the value adopted above, K band surface photometry becomes possible; an integration time of 3.0 hr is needed to achieve a signal-to-noise ratio of 3 at 3.4 scale lengths. We note that (i) many low redshift galaxies do have central surface brightnesses that are brighter than the standard value adopted in the previous paragraph; (ii) the intrinsic surface brightness of disks at $z = 1.7$ may well be higher than at $z = 0$, depending on their star formation history.

6.13.3 Guide Star Availability

This project can be done in any high latitude fields so galaxies will be selected based on proximity to suitable guide stars.

6.13.4 Special Requirements

Uniformity of the PSF over the GSAOI field is very desirable for deriving the surface brightness profiles.

6.14 Color Gradients in High Redshift Field Galaxies

6.14.1 Science Goal

The observational study of high redshift field galaxies is one of the major thrusts of current research. The goals are twofold:

- To take snapshots of the galaxy population at different cosmic epochs, and understand physically what we are seeing. For example, what are the fuzzy objects at $z = 3$ and why are they so blue?
- To tie these different snapshots together into a coherent picture of the history and evolution of the Universe. For example, will those fuzzy objects at $z = 3$ turn into a galaxy like our own?

Specific questions include:

- When did bulges form?
- Why are galaxy disks so much larger than predicted by CDM?
- How important are mergers?
- How and when were metallicity gradients established?

These goals are discussed in detail in the MCAO Science Case (RPT-AO-G0107). GSAOI can address them statistically using high spatial resolution imaging of a large sample of galaxies at a range of redshifts.

The bulge and disk luminosities and colors will be measured separately for each galaxy. The multivariate distribution function of these properties, as a function of redshift, will then be compared with the output of n -body and semi-analytic simulations to place limits on the formation and evolution physics.

The galaxy sample will need to be large (several hundred galaxies) to get reasonable statistics as a function of redshift since galaxies are diverse in their properties. The study must reach redshifts of $z > 0.5$ to probe sufficiently large look-back times to sample evolutionary effects.

A combination of high spatial resolution imaging and sensitive detection at near-infrared wavelengths is required to address the science goals.

Resolution: At redshifts above one, 1" corresponds to ~ 8 proper kpc, fairly independent of redshift. Thus significantly sub-arcsec resolution is needed to resolve most galaxies. In particular, unless the resolution is substantially better than 0.1", it is not possible to decompose galaxies into their disk and bulge components and measure their separate properties.

Near-infrared imaging: WFPC3 and ACS on HST will provide deep, high-resolution optical imaging of high redshift field galaxies. Near-infrared imaging with comparable resolution will be needed, for the following reasons:

- Short-lived O and B stars dominate the flux of most galaxies below rest-frame 400 nm. The ultra-violet flux is thus a measure of some combination of the instantaneous star formation rate and the dust obscuration. It tells us little or nothing about the older stellar population, metallicity, age, mass, etc. At redshifts above 1.5, observed-frame near-infrared imaging is thus needed to see beyond rest-frame 400 nm.
- Tying together observations at different redshifts requires observations at the same rest-frame wavelengths. *JHK* imaging allows us to observe galaxies in the rest-frame *B* band out to $z = 4$.
- Imaging at near-infrared wavelengths give us a view of galaxy morphology less affected by dust obscuration.

We have simulated the appearance of high redshift galaxies with GSAOI. Local galaxies were shifted to high redshifts, convolved with a MCAO PSF, and noise added. For a total (atmosphere, telescope, AO, imager, and detector) throughput of 25%, we should be able to perform accurate bulge-disk deconvolutions down to $K \sim 21.3$ mag, provided that the PSF is reasonably well known. At this limit, there will be around 30 galaxies in an $80'' \times 80''$ field, with a median redshift of $z \sim 1.2$. A sample of ~ 1000 galaxies will be required to get reasonable statistics across the whole range of morphologies and redshifts. Imaging each galaxy at *J* and *Ks* will require around ten nights observing.

If we can reach $K = 21$ mag, MCAO will have a multiplex advantage of around ten over conventional AO. In addition, the relative uniformity of the PSF across the GSAOI field will be very important in performing accurate bulge-disk decompositions, as documented in the MCAO Science Case. Thus large surveys of field galaxies will not be possible without MCAO.

NICMOS camera 3 has pixels that are too large for reliable bulge-disk decomposition. Cameras 2 and 1 have more suitable pixel sizes. Simulations of their performance relative to MCAO show that they do well in the central regions of galaxies but the high dark current and read noise badly affect the data a few tenths of an arcsec from the galaxy center. Our simulations suggest that MCAO will get suitable data for sources about 1 mag deeper than NIC2 in the *H* band. In addition, the fields-of-view of the NIC1 and NIC2 cameras (11" and 19", respectively) are too small to get more than one galaxy per pointing.

6.14.2 Sensitivity Limit

To get a useful multiplex advantage over conventional AO, we need to reach $K = 20$ mag or better, with exposure times of order one hour, and sufficient signal-to-noise ratio to measure color gradients and do a disk-bulge deconvolution. Our simulations suggest that this is achievable with a total throughput (including

atmosphere, telescope, AO, instrument and detector) of 25%. GSAOI is expected to exceed this requirement.

6.14.3 Guide Star Availability

This project can be carried out in any part of the high galactic latitude sky. There is no particular advantage in doing contiguous regions. Targets can thus be chosen based on the availability of suitable guide stars.

6.14.4 Special Requirements

Uniformity of the PSF across the field is important for the galaxy decomposition.

6.15 Exploring Dark Energy Via High Redshift Supernovae

6.15.1 Science Goal

Type Ia supernovae have emerged as one of the sharpest tools in the astrophysicist's shed for measuring extragalactic distances, with a precision of $\sim 6\%$. These exploding stars have shown, through observations made by the High-Z SN Search Team and the Supernova Cosmology Project that the Universe is accelerating in its expansion, a result that indicates the cosmos must be filled with some previously unknown form of dark energy. By studying Type Ia supernovae with GSAOI we can accurately trace the cosmic expansion to $z \sim 2$, learning key physical properties of the dark energy.

Different types of dark energy affect the rate at which the Universe expands depending on their effective equation of state. For example, the cosmological constant has an equation of state, $w \equiv p/\rho = -1$, where as quintessence – a scalar field – has $w > -1$. Each variant of dark energy has its own evolving equation of state that produces a signature in the Hubble diagram of the SNe Ia. With current instrumentation, we can find and follow SNe Ia to $z = 1.1$. To move beyond this redshift, we need an instrument with near-infrared sensitivity such as GSAOI.

Complementary optical spectral observations of the host galaxy are useful to accurately measure the redshift of the SN.

6.15.2 Sensitivity Limit

Table 12 lists the brightness at maximum light of a SN Ia as a function of redshift assuming a Lambda Cosmology ($\Omega_\Lambda = 0.7$, $\Omega_M = 0.3$). The integration time needed to adequately detect it with GSAOI is also tabulated. It is apparent that SNe can be measured in the H band to $z > 2$ using GSAOI.

To achieve an accurate (~ 0.2 mag) distance measurement, each SN must be observed in two bands at maximum light with a total signal-to-noise ratio of all observations combined > 20 . In addition, they should be followed for > 15 days in the rest frame at approximately five epochs with a signal-to-noise ratio > 5 , at which point they will be ~ 0.7 mag fainter than at maximum light. A sample of > 10 objects is required to adequately constrain the SN Ia Hubble diagram at $z > 1.1$. In total, this program will require approximately 40 nights of observing time.

Table 12: Predicted SN Ia Magnitudes

Redshift	SN Ia Brightness				GSAOI Imaging Time (hrs) ¹				Total Integration Time per SN ¹ (hrs)
	Z	J	H	K	Z	J	H	K	
1.2	23.8	23.6	23.6		0.2	1.4	1.4		14.5
1.3	24.2	23.8	23.7		0.3	2.1	1.7		19.5
1.4	24.5	23.9	23.7		0.6	2.5	1.7		22.0
1.5		24.1	23.7	23.8		3.6	1.7	3.6	28.7
1.6		24.3	23.8	23.9		5.2	2.1	4.4	30.0
1.7		24.5	23.9	24.1		7.6	2.5	6.3	40.3
1.8		24.6	23.9	24.2		9.1	2.5	7.6	45.4
1.9		24.8	24.1	24.2		13.2	3.6	7.6	52.1
2.0		24.9	24.2	24.2		15.8	4.4	7.6	56.5

¹Based on CoDR sensitivity estimates.

6.15.3 Guide Star Availability

Supernovae can be discovered either using HST+WFPC3/ACS in pre-selected locations that have guide stars. Recent work with HST has demonstrated that two images, separated by 1 month in the rest frame will yield 1 SN Ia per 50 square arcminutes to $z < 2$. A HST program with ACS can survey to $Z = 26$ mag in 3 orbits and therefore uncover 1 SN Ia to $z < 2$ per 15 orbits.

Alternatively, GSAOI could be used to search around pre-selected guide stars for very distant SNe Ia at $z \sim 2$ in the H band using its full $85'' \times 85''$ field-of-view; a perfect PSF is not necessary for SN discovery. The rate of discovery in this mode will be ~ 1 SN per ~ 40 hr of integration time. This could be achieved through utilizing observations from other programs as appropriate.

6.15.4 Special Requirements

A uniform PSF across the GSAOI field is required to accurately measure the SN photometry as it rises and falls in its brightness. The observations need broadband filters that are matched to their optical rest frame equivalent. For example, for a SN at $z = 1.9$, H band matches rest frame V band.

7 Setup and Calibration Requirements

7.1 Daytime GSAOI Setup and Calibration

Most GSAOI programs use a standard setup and require a basic set of calibration observations to be obtained during the afternoon prior to observing. These standard setup and calibration observations are described here. The MCAO startup and calibration is part of this setup, so those procedures for this that are described in the MCAO Operational Concept Definition Document are repeated here where appropriate. The various MCAO subsystems are the Adaptive Optics Module (AOM), Diagnostic Wave Front Sensor (DWFS), Laser System (LS), Beam Transfer Optics (BTO), Laser Launch Telescope (LLT), MCAO Control System (MCAO-CS), and Safe Aircraft Localization and Satellite Acquisition (SALSA) system. The AOM consists of the first Off-Axis Parabola (OAP-1), Deformable Mirrors DM2, DM1, and DM0, the Tip-Tilt Mirror (TTM), the Beam Splitter (BS1), the Atmospheric Dispersion Corrector (ADC), and the second Off-Axis Parabola (OAP-2).

7.1.1 GSAOI Bias and Dark Frames

GSAOI bias frames are obtained by selecting the "Blocked" position in the lower filter wheel and recording a sequence of minimum duration (5 s) exposures. Typically 10-15 such exposures each consisting of 12

coadds each (1 min of data) will be obtained so that cosmic ray events can be removed by median filtering during data reduction.

- Close the GSAOI environmental cover.
- Set the GSAOI lower filter wheel to the "Blocked" position.
- Set the GSAOI imager detector readout method to Fowler Sampling and load the appropriate timing file.
- Set the View Mode integration time to 5 s (the minimum), number of Fowler samples to 1, and number of coadds to 1.
- Set the Observe Mode integration time to 5 s, number of Fowler samples to 1, and number of coadds to 12.
- Record an Observe Mode bias frame.
- The bias frame is automatically displayed in the Observe Mode Quick Look Display.
- Load the bias frame as the View Mode Quick Look Display subtraction file; the subtracted frame is displayed.
- Load the bias frame as the Observe Mode Quick Look Display subtraction file; the subtracted frame is displayed.
- Set the Observe Mode repeats to 14.
- Record an Observe Mode sequence.
- The bias-subtracted bias frames are automatically displayed in the Observe Mode Quick Look Display.

Dark frames can be obtained by repeating the above sequence for each exposure time used for science observations.

- Close the GSAOI environmental cover.
- Set the GSAOI lower filter wheel to the "Blocked" position.
- Set the GSAOI imager detector readout method to Fowler Sampling and load the appropriate timing file.
- Set the View Mode integration time to 5 s, number of Fowler samples to 1, and number of coadds to 1.
- Load the previous bias frame as the View Mode Quick Look Display subtraction file; the subtracted frame is displayed.
- Set the Observe Mode integration time to an appropriate value, say 60 s, number of Fowler samples to 3, and number of coadds to 1.
- Load the previous bias frame as the Observe Mode Quick Look Display subtraction file; the subtracted frame is displayed.
- Set the Observe Mode repeats to 5.
- Record an Observe Mode sequence.
- The bias-subtracted dark frames are automatically displayed in the Observe Mode Quick Look Display.

7.1.2 MCAO AOM Calibrations

- Measure the bias and read noise levels in each wave front sensor (WFS) CCD.
- Insert the LGS reference source flip mirrors, turn on the reference sources, and center them in the fields-of-view of the higher-order WFSs. Measure and store the reference gradients sensed by each WFS for a known flat wave front at the WFS. Measure WFS gains and tilt transfer functions by scanning the reference sources.
- Set the figure of each deformable mirror using previously calibrated actuator commands, cycling the mirror if necessary to avoid hysteresis effects (these commands do not necessarily flatten the mirrors, but should produce a corrected wave front at the science instrument). Center the TTM. Insert the simulated NGS sources. Adjust the TTM and focus on DM1 to null the tip-tilt/focus measurements from the relevant MCAO WFS. Insert the DWFS, and measure wave front quality across the field.
- Insert and turn on the simulated LGS sources. Measure and store the gradients sensed by each LGS WFS for the calibrated DM actuator commands. Repeat at several LGS ranges.

- Close the tip-tilt and higher-order AO control loops to verify stability.
- Open the tip-tilt and higher-order AO control loops.
- Turn off the LGS reference sources and retract the LGS reference source flip mirrors.
- Turn off and retract the simulated NGS sources.
- Retract the DWFS.

- Insert the simulated NGS sources.
- Open the GSAOI environmental cover.
- Set the GSAOI upper filter wheel to the *H* filter.
- Set the GSAOI lower filter wheel to the "Clear" position.
- Set the GSAOI utility wheel to the convex defocus lens.
- Record an Observe Mode image.
- Set the GSAOI utility wheel to the concave defocus lens.
- Record an Observe Mode image.
- Process the two images with *the ExtraFocal* program.
- Enter Zernike coefficients to deform the MCAO DM0 to correct non-common path wave front errors due to the GSAOI imager.

7.1.3 GSAOI Flat Field Frames

There are three ways in which GSAOI flat field frames could be recorded; exposures of the "Black Body" lamp in the Gemini Calibration Unit (GCAL), exposures of the illuminated dome interior, and exposures of the sky. The first of these (i.e., GCAL exposures) suffer from the fact that the GCAL beam is introduced via the ISS science fold mirror and so does not include the effects of the MCAO optics. Lamp-on minus lamp-off exposures of the dome interior are the best way of recording the response of the telescope/MCAO/GSAOI system to transmitted light. The large number of warm optical elements in MCAO means that their thermal emission is likely to be significant in single exposures. Sky exposures offer the advantages of being recorded through the full optical system and at the same time as the science observation. However, the thermal emission component from the warm optics cannot be removed. This unknown offset leads to an erroneous determination of the relative pixel sensitivities.

The true instrumental response will be measured using star exposure grids during commissioning. This will be used to define the preferred flat fielding procedure. Experience in flat fielding AO images will also be obtained with ALTAIR and NIRI. For now, we describe a procedure for recording lamp-on/lamp-off exposures of the dome interior. The minimum exposure time of 5 s will typically be used with typically 12 coadds for a total integration time of 60 s.

- Deploy the AO fold and science fold mirrors, and command the MCAO deformable mirrors to their nominal figures.
- Open the MCAO shutters.

- Open the GSAOI environmental cover.
- Set the GSAOI upper filter wheel to the *Ks* filter position.
- Set the GSAOI lower filter wheel to the "Clear" position.
- Set the GSAOI utility wheel to the "Clear" position.
- Set the GSAOI detector readout method to Fowler Sampling and load the appropriate timing file.
- Set the View Mode integration time to 5 s (the minimum), number of Fowler samples to 1, and number of coadds to 1.
- Load the previous bias frame as the View Mode Quick Look Display subtraction file; the subtracted frame is displayed.
- Set the Observe Mode integration time to 5 s, number of Fowler samples to 1, and number of coadds to 12.
- Set the Observe Mode repeats to 5.

- Load the previous bias frame as the Observe Mode Quick Look Display subtraction file; the subtracted frame is displayed.
- Slew the telescope to point to an appropriate place on the dome interior.
- Switch dome lights OFF.
- Record an Observe Mode sequence.
- The bias-subtracted lamp-OFF frames are automatically displayed in the Observe Mode Quick Look Display.
- Load a lamp-OFF frame as the Observe Mode Quick Look Display subtraction file; the subtracted frame is displayed.
- Switch dome lights ON.
- Record an Observe Mode sequence.
- The lamp-OFF-subtracted lamp-ON frames are automatically displayed in the Observe Mode Quick Look Display.
- Repeat for other filters as required.

7.1.4 MCAO Laser Startup

The startup procedure for the Laser System is **TBD**.

7.2 Nighttime GSAOI Setup and Calibration

7.2.1 Twilight GSAOI Flat Field Frames

The three methods of recording flat field frames were listed in §7.1.3. It is desirable to obtain high signal-to-noise ratio sky flats to complement dome flats. Twilight sky flats can be recorded with the same setup used in §7.1.3.

7.2.2 Nighttime MCAO Calibration

The primary purpose of the nighttime MCAO calibration sequence is to establish a common bore sight reference between the BTO and GSAOI. AO loop performance may also be characterized on a known reference field if desired. This operation should not take more than 5 minutes once the telescope is on the object, and eventually should be fully automated as an observing script. The sequence starts with the laser running and all laser shutters closed.

- Open the laser shutter at the LS/BTO interface. Close each beam pointing and centering loop through the BTO in sequence, using images from the pre-alignment cameras as necessary. Verify beam pointing, centering, quality, and power for each beam using the diagnostic sensors. Open the pointing and centering loops, and close the laser shutter at the LS/BTO interface. These operations may be performed at the end of the day.
- Open the LLT dust cover.
- Slew the telescope to a reference star. The active optics PWFS1 guide star is acquired and the telescope's tracking and active optics are enabled. The SALSA and internal safety systems are operating.
- Initiate MCAO-CS control of the BTO centering mirror (CM), pointing mirror (PM), and de-rotation K-mirror (KM). These elements are positioned using a lookup table with the telescope pointing angle as input.
- Deploy the AO fold and science fold mirrors, and command the deformable mirrors to their nominal figures.
- Acquire the reference star with the ODGW. Switch telescope tip-tilt control from PWFS1 to the ODGW, and track using the TTM and M2.
- The reference star is now imaged or sensed by the BTO beam near- and far- field diagnostic sensors. Adjust PM and CM so that the star images are correctly centered. Move the BTO corner cube shutter to the closed position.

- Open the laser shutter at the LS/BTO interface. Close each beam centering and pointing loop through the BTO in sequence. Verify beam pointing, centering, quality, and power for each beam and polarization at the diagnostic sensor.
- Zoom the LGS WFS to focus at the nominal range for the current elevation angle.
- Open the laser beam dump shutter in the BTO to propagate the laser to the sky, and verify that signal is detected from each guide star at the LGS WFS.
- Shutter the laser, open the ODGW tracking loop, and proceed to the first observation.

7.2.3 Nighttime GSAOI Flux Calibration

GSAOI flux calibration will be achieved in the usual way by recording images of standard star fields. The procedure for acquiring a science field is described in §7.3.

7.2.4 Nighttime GSAOI Geometrical Distortion Calibration

Proper mosaicing of GSAOI imager frames will require accurate registration of both the four individual GSAOI imager detector frames and any dithered mosaic sets. The correct registration of the four imager detector frames can be achieved by recording exposures of suitable astrometric reference fields.

7.3 MCAO Science Field Acquisition

Acquisition of the science field with MCAO is a routine setup procedure that will be described only once here. The science field is observed with the acquisition camera to determine the precise locations and magnitudes of the guide stars for the MCAO NGS WFS and the ODGW. This information is used to compute the MCAO control algorithm and position the NGS WFS probe arms.

A guide star in any one of the four imager On-Detector Guide Windows can be used for slow tip-tilt (flexure) correction. The square guide window is specified by selecting the window size (8×8, 12×12, 16×16, 32×32) and defining its center. This can be determined either from the acquisition camera frame or directly from an imager detector exposure of the science field.

Target acquisition should take a maximum of 2 minutes, and should eventually be automated as part of the observing script.

The AO fold and science fold mirrors are already deployed. The GSAOI environmental cover is open, and all GSAOI mechanisms are in their observing positions.

- Slew the telescope to the science object coordinate.
- The instrument rotator position angle is set during the slew, and subsequently maintained at this angle.
- Set PWFS1, the MCAO NGS WFS, and the ODGW to the absolute positions of their respective guide stars.
- Select PWFS1 as the primary tracking reference.
- PWFS1 acquires its guide star and begins active correction.
- Shutter the laser at the LS/BTO interface.
- The BTO pointing, centering, orientation, and polarization control elements are set to their nominal (calibrated) values for the current zenith angle.
- The SALSA and internal laser safety systems are operating.
- Command the deformable mirrors to their nominal figures.
- Acquire the MCAO NGS WFS guide stars.
- Zoom the LGS WFS to focus at the nominal range of the sodium layer for this elevation angle.
- Open the laser shutter at the LS/BTO interface. Close each beam centering and pointing loop through the BTO in sequence. Verify beam pointing, centering, quality, and power for each beam and polarization at the diagnostic sensor, and also the orientation of the LGS constellation. Verify that signal is detected on the LGS WFS.
- Close the high bandwidth BTO tip-tilt loops to center the LGS spots on the LGS WFS.

- Switch to tracking using the MCAO NGS WFS. Close the DM control loop using the MCAO WFSs.
- Acquire the ODGW guide star.
- Close the supervisory control loop for the NGS WFS bore sight using the ODGW tip-tilt measurements as input.
 - Long-term drift/flexure is tracked using the ODGW, the MCAO TTM, and M2.
 - The NGS WFS locations are adjusted to center the average guide star position on each sensor.
 - This compensates for any residual uncertainty in the positions of the guide stars.
 - It could take up to 1 min to average out turbulence effects in the ODGW guide star position.
- Perform the science instrument integration.
 - ODGW read outs stop while the initial full-frame detector read outs occur.
 - ODGW read outs then resume – the supervisory control loop must bridge this gap.
 - ODGW read outs stop while the final full-frame detector read outs occur.
 - ODGW read outs then resume – the supervisory control loop must bridge this gap.
 - AO performance can be monitored using the output displayed by several of the supervisory loops (estimated PSFs, open- and closed-loop turbulence statistics, LGS signal level,...).
- Open the DM control loops and return to tracking using only the NGS WFS. Open the BTO control loops, and shutter the laser at the LS/BTO interface. Open the NGS WFS tracking loop and proceed to the next observation.

7.4 Nightly Shutdown

7.4.1 GSAOI Shutdown

GSAOI should be left in a safe configuration at the end of observing.

- Close the GSAOI environmental cover.
- Set the GSAOI lower filter wheel to the "Blocked" position.

7.4.2 MCAO AOM Shutdown

- Open the DM control loops. Open the BTO control loops, and shutter the laser at the LS/BTO interface. Open the NGS WFS tracking loop.
- Close the MCAO shutters.

7.4.3 MCAO Laser Shutdown

The shutdown of the LS should be automated and transparent to the end user.

8 Observing Scenarios

A typical actual observing scenario is described in this section in order to elaborate on the science descriptions in §6 and to identify and illuminate the requirements GSAOI places on other parts of the Gemini telescope system.

8.1 Evolution of Dwarf Irregular Versus Elliptical Galaxies

8.1.1 Scientific Background

Small galaxies are classified as one of two types; dwarf ellipticals and dwarf irregulars. Not only their appearance, but also some of their fundamental properties (e.g., gas content, star formation history, *M/L* ratios) are dramatically different. Does the environment play a role in governing the star formation history of dwarf elliptical galaxies? Is there an evolutionary link between dwarf ellipticals and dwarf irregulars?

The Milky Way companion dwarf ellipticals (called dwarf spheroidals for historical reasons) show a variety of star formation histories. These vary from "basically old" (ages greater than about 10 Gyr) to "dominated

by intermediate-age" (from 2 to about 10 Gyr). The star formation histories also vary in their details. In some cases, they show obvious "episodes" of star formation separated by quiescent periods, while in other cases it appears that continuous star formation has occurred. At present there is little understanding of this diversity. However, there are a number of distinctive features of the Local Group dwarf galaxies as follows:

- One important clue may be a "correlation" with the distance from the Milky Way: the dwarf ellipticals with larger intermediate-age fractions are generally at larger distances. This hints at the influence of parent galaxy/environment. Possible factors include tidal influence, Galactic winds, ram pressure stripping, high X-ray or UV flux; in short, anything that might affect gas content evolution or conditions for early star formation.
- In the M31 system, at least for the lower luminosity dwarf ellipticals (i.e., not NGC 147/185/205), the situation is strikingly different. The intermediate-age populations are less obvious compared to the Milky Way's companions; e.g., there is no system near M31 known to have a population younger than approximately 5 Gyr, whereas there are at least 3 Galactic companions with ~ 1 -3 Gyr populations. Also, the system with the youngest intermediate-age population (~ 6 -8 Gyr) is the most distant from M31.
- There are low-luminosity galaxies, mostly dwarf irregulars or transition objects, in the Local Group that are not directly associated with the Galaxy or M31 (e.g., WLM, LGS3, and Phoenix). All contain young stars and varying amounts of H I. This again hints at some effect from the environment, but the fact that the isolated dE Tucana contains only old stars indicates that this cannot be the complete story.
- Two dwarf ellipticals in the M81 group, which is a much more compact environment than the Local Group, have been studied with HST. Both systems show strong upper-AGB populations; i.e., stars more luminous than those of the red giant branch tip. This by itself is an indication of a significant intermediate-age population. The intermediate-age populations in Galactic dwarf ellipticals were actually first recognized via identification of the upper-AGB (carbon) stars.

8.1.2 Proposed Observations

The plan is to measure J , K magnitudes for the upper-AGB stars in dwarf ellipticals beyond the Local Group. This should give bolometric magnitudes that in turn yield age estimates (the luminosity at the AGB-tip is higher for younger systems). Near-infrared measurements are an advantage for these studies since variability (all upper-AGB stars are variable at some level) is much less in the near-infrared than in the optical. The sensitivity limit of NIRI (and FLAMINGOS-I/II) allows surveying dwarf ellipticals just beyond the Local Group with long integration times per galaxy. However, to go beyond this requires the fainter limiting magnitudes that only MCAO/GSAOI can provide. In the southern hemisphere, the dwarf ellipticals in the Centaurus group and in the most distant part of the Sculptor Group are prime targets. Going further in distance, there is the loose association of galaxies that contain the Circinus galaxy at a distance of 6-7 Mpc, the Leo I Group, and perhaps the Virgo and Fornax galaxy clusters.

We focus on J and K_s observations of the Centaurus A group dwarf elliptical ESO219-010 (Jerjen, Freeman, & Binggeli 2000).

8.1.3 Planning the Observation

Celestial coordinates for ESO219-010 are obtained from Jerjen et al. The Perl script *gs_search.pl* is used to plan the observation. This retrieves and displays DSS, 2MASS, WFPC2, and NICMOS images of the field. In the case of ESO219-010, only a red DSS-2 image and the 2MASS K band image are available. The DSS-2 image is shown in Figure 14. The object is offset from the field center to avoid the gaps between each detector. The object will be positioned within each imager detector quadrant in order to maximize the on-source integration time and to measure the sky flux accurately. The coordinates of the four field centers are listed in Table 13. The dither spacing must be at least as large as the PSF wings of the bright stars within the science field. The low Galactic latitude of ESO219-010 makes MCAO NGSs abundant. We choose U0375_16981750 ($R = 15.0$ mag), U0375_16981181 ($R = 17.1$ mag), and U0375_16978938 ($R = 17.6$ mag). These three stars are distributed in an appropriate triangle about ESO219-010. The ODGW guide star

is marked by a small yellow circle in each frame of Figure 14. We use U0375_16981750, the $R \sim 15.0$ mag NGS, although its near-infrared magnitudes are yet to be determined.

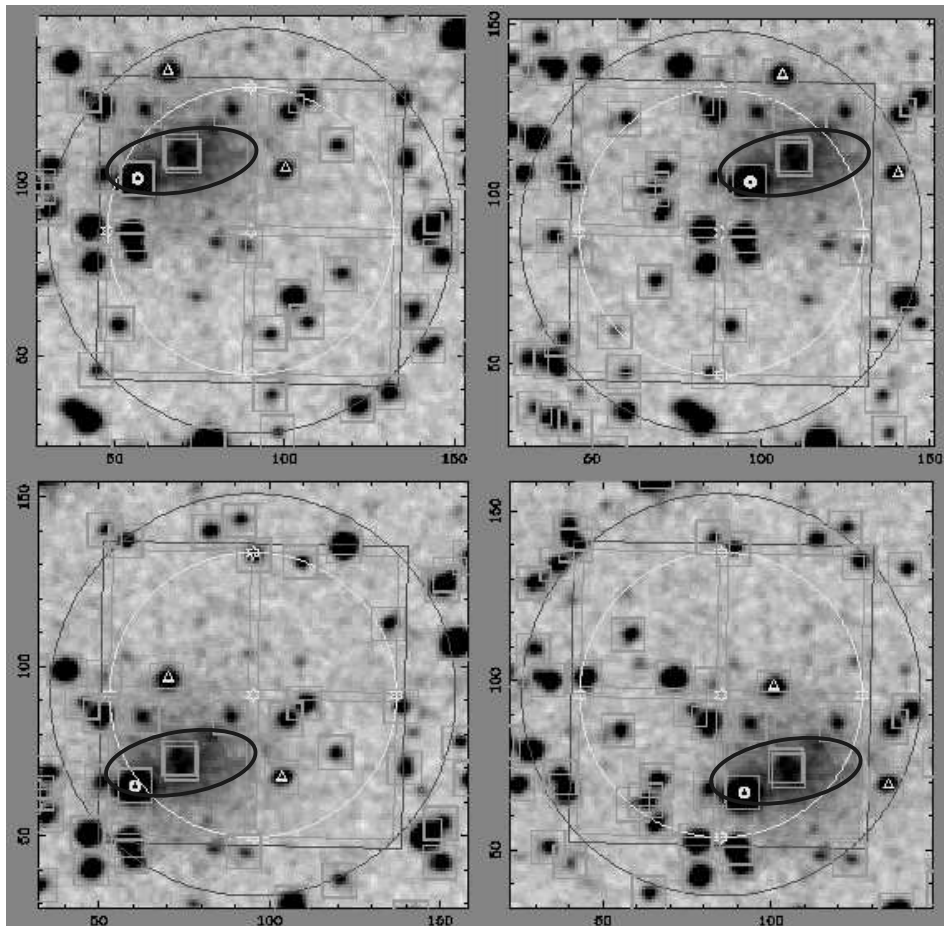


Figure 14: Plan for ESO219-010 observation made with *gs_search.pl*. The DSS-2 image of ESO219-010 is shown as a grayscale. The blue ellipse indicates the object. The fields of the four GSAOI imager detectors are shown in green. A red circle indicates the 2' diameter MCAO field. A red square marks the outline of the GSAOI field mask. The LGS constellation is shown in yellow. US Naval Observatory catalog stars are enclosed in orange boxes. The three NGS selected are marked by yellow triangles. A small yellow circle marks the ODGW guide star.

Table 13: Field Centers for ESO219-010 Observation

Quadrant	RA (J2000)	Dec
1	12:56:07.7	-50:08:58
2	12:56:12.1	-50:08:58
3	12:56:07.7	-50:08:15
4	12:56:12.1	-50:08:15

8.1.4 Daytime Calibrations

The standard daytime calibration procedure will be followed, including recording GSAOI imager bias and dark frames and dome flat field frames. These procedures are described in §7.1.

8.1.5 Nighttime Calibrations

Twilight sky flat field frames will be obtained as described in §7.2.1 above. An astrometric field will be measured to define the geometrical distortion calibrations for each imager detector and their relative offsets. This procedure is described in §7.2.4 above. Nearby flux standard star will be measured in both the *J* and *K* filters before and after the science exposures. This procedure is described in §7.2.3 above.

8.1.6 Setup Prior to Observation

The observation setup consists of the following actions:

- Open the GSAOI environmental cover.
- Set the GSAOI upper filter wheel to the *Ks* position.
- Set the GSAOI utility wheel to the "Clear" position.
- Set the GSAOI lower filter wheel to the "Blocked" position to avoid saturating the imager detector.
- Slew telescope to the first field center coordinate.
- The instrument rotator is set to 0° position angle on the sky during the slew, and subsequently maintained at this angle.
- The AO feed mirror and ISS science fold mirror are deployed.
- The MCAO shutters are open.
- Set PWFS1, the MCAO NGS WFSs, and ODGW to the absolute positions of their respective guide stars.
- Set the GSAOI imager detector readout method to Fowler sampling and load the appropriate timing file.

When the telescope has settled:

- Set the GSAOI lower filter wheel to the "Clear" position.

Begin active and adaptive correction as described in §7.3 above.

- Set the View Mode integration time to 5 s, number of Fowler samples to 1, and number of coadds to 1.
- Set the Observe Mode integration time, number of Fowler samples, and number of coadds to the View Mode values.
- Load a previous bias frame as the Observe Mode Quick Look Display subtraction file; the subtracted frame is displayed.
- Offset the telescope to a sky position 2' north.
- Wait for the telescope to settle.
- Record an Observe Mode exposure.
- The bias-subtracted frame is automatically displayed in the Observe Mode Quick Look Display.
- Load the sky frame as the View Mode Quick Look Display subtraction file; the subtracted frame is displayed.
- Offset the telescope back to the first field center coordinate.
- Wait for the telescope to settle.
- Resume active and adaptive correction.
- The sky-subtracted imager field is continuously updated in the View Mode Quick Look Display.

8.1.7 Science Observation Sequence

Record pre-observation bias frame:

- Set the Observe Mode integration time to 5 s (the minimum), number of Fowler samples to 1, and number of coadds to 12.
- Set the GSAOI lower filter wheel to the "Blocked" position.

- Record an Observe Mode bias frame.
- The bias-subtracted bias frame is automatically displayed in Observe Mode Quick Look Display.
- Load the bias frame as the Observe Mode Quick Look Display subtraction file; the subtracted frame is displayed.
- Set the GSAOI lower filter wheel to the "Clear" position.

Perform science observation sequence:

- Set the Observe Mode integration time to 60 s, number of Fowler samples to 8, and number of coadds to 1 for a 60 s integration.
- Record an Observe Mode exposure.
- The bias-subtracted frame is automatically displayed in the Observe Mode Quick Look Display.
- Load the object frame as the Observe Mode Quick Look Display subtraction file; the subtracted frame is displayed.
- Offset the telescope to the second field center coordinate.
- Wait for the telescope to settle.
- Resume active and adaptive correction.
- Record an Observe Mode exposure.
- The sky-subtracted frame is automatically displayed in the Observe Mode Quick Look Display.
- Offset the telescope to the third field center coordinate.
- Wait for the telescope to settle.
- Resume active and adaptive correction.
- Record an Observe Mode exposure.
- The sky-subtracted frame is automatically displayed in the Observe Mode Quick Look Display.
- Offset the telescope to the fourth field center coordinate.
- Wait for the telescope to settle.
- Resume active and adaptive correction.
- Record an Observe Mode exposure.
- The sky-subtracted frame is automatically displayed in the Observe Mode Quick Look Display.
- Repeat sequence on a 0.5" dither grid as required.

Record post-observation bias frame:

- Set the Observe Mode integration time to 5 s (the minimum), number of Fowler samples to 1, and number of coadds to 12.
- Set the GSAOI lower filter wheel to the "Blocked" position.
- Load the pre-observation bias frame as the Observe Mode Quick Look Display subtraction file; the subtracted frame is displayed.
- Record an Observe Mode bias frame.
- The bias-subtracted bias frame is automatically displayed in Observe Mode Quick Look Display.
- Load the bias frame as the Observe Mode Quick Look Display subtraction file; the subtracted frame is displayed.

9 Summary of Scientific Requirements

The science programs discussed above lead to the following science requirements for GSAOI.

9.1 MCAO Compatibility

REQ-OCD-0001: GSAOI will accept the MCAO f/34 input beam with a pupil near the telescope secondary mirror.

9.2 Imager

REQ-OCD-0002: GSAOI will have an imager channel for science observations.

9.3 Imager Wavelength Coverage

REQ-OCD-0004: The imager will operate in the wavelength range from 0.9-2.4 μm .

9.4 Imager Spatial Sampling

REQ-OCD-0005: The imager will have a scale of $\sim 0.02''/\text{pixel}$.

9.5 Imager Field-of-View

REQ-OCD-0006: The imager will have a field-of-view of $> 80'' \times 80''$.

9.6 Imager Cold Stop

REQ-OCD-0007: The imager will include a fixed cold stop at an image of the MCAO exit pupil. The cold stop will be sized so as not to vignette the imager beam while reducing background radiation to the greatest extent possible.

9.7 Imager Pupil Viewer

REQ-OCD-0008: The imager will have a facility for viewing an image of the MCAO exit pupil.

9.8 Imager Non-Common Path Phase Errors

REQ-OCD-0009: The imager will be capable of measuring low-order wave front errors through the entire optical path to the imager detector with a spatial resolution of ~ 200 mm referenced to the telescope primary mirror.

9.9 Imager Filter Suite

REQ-OCD-0010: The imager will be able to interchange between any of the following filters:

Item	Filter	λ_c (μm)	$\Delta\lambda$ (μm)	50% cut on	50% cut off
1	Z	1.015	0.170	0.930	1.100
2	J	1.250	0.160	1.170	1.330
3	H	1.635	0.290	1.490	1.780
5	K'	2.120	0.340	1.950	2.290
6	Ks	2.150	0.320	1.990	2.310
7	K	2.200	0.340	2.030	2.370
7	J continuum	1.207	0.018	1.198	1.216
8	H continuum	1.570	0.024	1.558	1.582
9	CH ₄ (short)	1.580	0.100	1.530	1.630
10	CH ₄ (long)	1.690	0.100	1.640	1.740
11	Ks continuum	2.093	0.031	2.078	2.108
12	Kl continuum	2.270	0.034	2.253	2.287
13	He I 1.0830 μm	1.083	0.016	1.075	1.091
14	H I P γ	1.094	0.011	1.089	1.100
15	H I P β	1.282	0.019	1.272	1.292
16	[Fe II] 1.644 μm	1.644	0.025	1.631	1.656
17	H ₂ O	2.000	0.080	1.960	2.040
18	He I (2p2s)	2.058	0.031	2.042	2.073
19	H ₂ 1-0 S(1)	2.122	0.032	2.106	2.138
20	H I Br γ	2.166	0.032	2.150	2.182
21	H ₂ 2-1 S(1)	2.248	0.034	2.231	2.265
22	CO $\Delta v=2$	2.360	0.080	2.320	2.400

9.10 Imager Calibration

REQ-OCD-0011 The imager filter mechanism will contain one blocked position for recording bias frames.

9.11 Imager Pupil Viewer Resolution

REQ-OCD-0012 The imager pupil viewer will have a resolution of < 100 mm equivalent at the Gemini telescope primary mirror.

9.12 Imager Strehl Ratio

REQ-OCD-0013: The total wave front error introduced by the imager optical system will be < 65 nm RMS over the wavelength range 0.9–2.4 μm . This corresponds to a Strehl ratio of > 0.94 at a wavelength of 1.6 μm .

REQ-OCD-0013a: GSAOI shall have a uniform point spread function across its field-of-view such that the Strehl ratio does not vary by more than 0.01 at a wavelength of 2.2 microns.

9.13 Imager Distortion

REQ-OCD-0014: The imager will cause a geometrical distortion at the detector of < 0.1%.

9.14 Imager Throughput

REQ-OCD-0015: The imager will have a throughput over its required wavelength range of $\geq 50\%$ including the imager optics and filter, but not including the detector or throughput of the atmosphere, telescope, or MCAO science path.

9.15 Imager Instrumental Background

REQ-OCD-0016: The imager will have an internal instrument background less than either the natural background from the observed science field or the dark current of the detector whichever is greater.

9.16 Imager Ghost Images

REQ-OCD-0017: Ghost images generated in the imager optics must be at a level below 10^{-5} of the parent image.

9.17 Imager Sensitivity

REQ-OCD-0018: The imager will be capable of detecting point sources with $K = 23.0$ mag in 3600 s with a signal-to-noise ratio of 10 through a $0.08'' \times 0.08''$ aperture.

9.18 Imager Pupil Viewer Sensitivity

REQ-OCD-0019: The imager pupil viewer will be capable of detecting the expected background emission in the K band with a signal-to-noise ratio of > 10 in a 1 min integration.

9.19 Mechanism Set Time

REQ-OCD-0031: Individual GSAOI mechanisms should be set within 30 s.

9.20 Mechanism Configuration Time

REQ-OCD-0032: A complete reconfiguration of the GSAOI instrument should be achieved in < 1 min.

9.21 Imager Utility Wheel

REQ-OCD-0034: The imager will have a utility wheel for interchanging the following elements:

No.	Utility Wheel Contents
1	Clear
2	Pupil viewer
3	Convex defocus lens
4	Concave defocus lens

9.22 Imager On-Detector Guide Window

REQ-OCD-0038: The imager will have a facility for defining and processing data from a rectangular guide window on the imager detector that will be used for monitoring tip-tilt motion due to flexure variations between MCAO and GSAOI, and for performing fast tip-tilt sensing when substituting for one of the MCAO NGS sensors.

9.23 Imager Detector Read Noise

REQ-OCD-0039: The imager detector will employ read noise reduction techniques, such as Fowler sampling, to achieve an effective read noise of < 10 e.

9.24 Imager Detector Dark Current

REQ-OCD-0040: The imager detector will have a dark current $< 0.1 \text{ e s}^{-1} \text{ pix}^{-1}$.

9.25 Imager On-Detector Guide Window Performance

REQ-OCD-0041: The imager On-Detector Guide Window should be able to determine the centroid of a star with $K < 19$ mag to an RMS accuracy of 1/10 of the image full width at half maximum in a 30 s exposure and sense tip-tilt corrections in 0.01 s exposures on stars with $K < 11$ mag.

REQ-OCD-0041a: Tracking performance using the On-Detector Guide Window will result in < 0.1 pixel tracking error in the detector per 15 degree attitude change in the instrument.

9.26 Downtime

REQ-OCD-0042: GSAOI will have a downtime of $< 2\%$ scheduled time on the telescope and where possible, component failure shall result in gradual performance degradation.

9.27 Observing Modes

REQ-OCD-0043: GSAOI will support a View mode for acquiring temporary imaging data and an Observe mode for acquiring archived imaging data.

10 References

- Arnold, R., & Gilmore, G. 1992, MNRAS, 257, 225
Baraffe, I., Chabrier, G., Allard, F., & Hauschildt, P. H. 2002, A&A, 382, 563
Brandl, B., Brandner, W., Eisenhauer, F., Moffat, A. F. J., Palla, F., & Zinnecker, H. 1999, A&A, 352, L69
Côté, P., Welch, D. L., Fischer, P., & Irwin, M. J. 1993, ApJ, 406, L59
Dayal, A., Latter, W. B., Beiging, J. H., Meakin, C., Kelly, D. M., Hora, J. L., & Tielens, A. G. G. M. 2000, in Asymmetrical Planetary Nebulae II: From Origins to Microstructures, eds. J. H. Kasner, N. Soker, & S. Rappaport, ASP Conf. Ser., 199, 221
Freedman, W., et al. 2001, ApJ, 553, 47
Ibata, R. A., Gilmore, G., & Irwin, M. J. 1994, Nature, 370, 194
Jensen, J. B., Tonry, J. L., Thompson, R. I., Ajhar, E. A., Lauer, T. R., Rieke, M. J., Postman, M., & Liu, M. C. 2001, ApJ, 550, 503
Jerjen, H., Freeman, K. C., & Binggeli, B. 2000, AJ, 119, 166
Kalirai, J. S., Ventura, P., Richer, H., Fahlman, G. G., Durrell, P. R., D'Antona, F., & Marconi, G. 2001, AJ, 122, 3239
Lucas, P. W., Roche, P. F., Allard, F., & Hauschildt, P. H. 2001, MNRAS, 326, 695
Lynden-Bell, D. 1976, MNRAS, 174, 695
Lynden-Bell, D., Faber, S. M., Burstein, D., Davies, R. L., Dressler, A., Terlevich, R. J., & Wegner, G. 1988, ApJ, 326, 19
Lynden-Bell, D., & Lynden-Bell, R. M. 1995, MNRAS, 275, 429
Majewski, S. R., Munn, J. A., & Hawley, S. L. 1994, ApJ, 427, L37
Monet, D. G., Dahn, C. C., Vrba, F. J., Harris, H. C., Pier, J. R., Luginbuhl, C. B., & Ables, H. D. 1992, AJ, 103, 638
Persson, S. E., Murphy, D. C., Krzeminski, W., Roth, M., & Rieke, M. J. 1998, AJ, 116, 2475
Roddier, C., & Roddier, F. 1993, JOSA, 10, 2277
Searle, L., & Zinn, R. 1978, ApJ, 225, 357
Soria R., et al. 1996, ApJ, 465, 79
Tinney, C. G. 1996, MNRAS, 281, 644
Tinney, C. G., Reid, I. N., Gizis, J., & Mould, J. R. 1995, AJ, 110, 3014
Tinney, C. G., Da Costa, G. S., & Zinnecker, H. 1997, MNRAS, 285, 111
Tinney, C. G. 1999, MNRAS, 303, 565
Tonry, J. L., Blakeslee, J. P., Ajhar, E. A., & Dressler, A. 2000, ApJ, 530, 625
van den Bergh, S. 1993, AJ, 107, 971
Vassiliadis, E., Dopita, M. A., Meatheringham, S. J., Bohlin, R. C., Ford, H. C., Harrington, J. P., Wood, P. R., Stecher, T. P., & Maran, S. P. 1998, ApJ, 503, 253

- Welch, C. A., Frank, A., Pipher, J. L., Forrest, W. J., & Woodward, C. E. 1999, ApJ, 522, L69
Wood, P. R., Bessell, M. S., & Fox, M. W. 1983, ApJ, 272, 99
Zinn, R. 1993, in The Globular Clusters- Galaxy Connection, ed. G. H. Smith & J. P. Brodie, ASP Conf. Ser., 48, 38